CHARACTERIZATION OF BIOCHAR DERIVED FROM DEMINERALIZED POULTRY LITTER IN TERMS OF ITS CANDIDACY TOWARDS ALTERNATIVE SOLID FUEL

Kevin Nyoni, Leungo Kelebopile

Botswana International University of Science and Technology, Palapye, Botswana, kevinnyoni57@gmail.com

An increase in global energy demand results in coal dependence which contributes to greenhouse gas emissions. Poultry litter (PL) is a potential substitute, but its poor physicochemical and combustion properties reduce its combustion efficiency; hence, demineralization and pyrolysis to biochar value-adds. The study analyzed the characterization of biochar derived from demineralized PL and selected the best-suited combustion technology. The PL was mechanically fractioned (4 mm) and leached in deionized water and pyrolyzed (300 °C; 15 min). The biochar physicochemical properties improved the higher heating value (22.31 MJ.kg^{-1}) and reduced the Ash Content (18.63 %) compared with undemineralized biochar. Increase in TGA/DTG heating rate shifted the reaction region to high temperature (58.57–548.93 °C) reducing the ease of ignition and combustion. The biochar has high fouling and slag tendency, and the fluidized bed combustion chamber was the preferred combustion technology. Mass of air at 7.83 kg kg^{-1} fuel is required to combust the biochar and produce 3.26 kg kg^{-1} fuel of flue gas. Flue gas produced with 25 % excess air produced a higher enthalpy than stoichiometric conditions, attaining a thermal efficiency of 86.20 %. Demineralized PL biochar exhibits excellent physicochemical and combustion properties making it an ideal fuel candidacy.

Key words: Biochar, Combustion properties, Demineralized poultry litter, Fluidized bed combustion, Physicochemical characterization, Thermal behavior.

Received 25/11/2025, Accepted 18/12/2025

1. Introduction

Over the past 75 yrs (1950 – 2025), the global population has increased from 2.54 billion to 8.18 billion with an annual compound growth rate (CAGR) of 1.57 % forecasting a population size of 9.74 billion by 2050 [1]. This increase in population size resulted in demand for energy, in which the primary energy consumption increased by 8.63 % yr^{-1}, reaching 186 383 TWh from 1990-2023 [2]. Fossil fuels are dominate in the supply of energy, occupying a fraction of 81.50 %, in which coal accounts for 32 % of that fraction. Coal dominates a large fraction of the global energy supply, which results in emission of carbon dioxide gas (CO_2) constituting a 41 % fraction of the global greenhouse gas emissions 57.40 $GtCO_2e$ [3]. This CO_2 gas is trapped in the atmosphere, which results in an increase in global temperature on average of 1.55 °C above the pre-industrial level (1850 yr), resulting in global warming [4]. Such an increase in global warming results in extreme weather conditions, such as little to no rainfall or floods, shifting the weather pattern. The continuous use of coal will further increase global warming, resulting in a projected temperature increase of up to 2.90 °C by the year 2100 as noted under the Paris Agreement [5]. Hence, an alternative renewable biomass that is carbon neutral and abundance is relevant to contribute to global warming mitigation, therefore Poultry Litter (PL) has the potential to be utilized and explored for potential use as a combustion solid fuel.

The Global Poultry industry per year produces 70.00 billion birds which resulting in Poultry Litter (PL) as waste, with an estimate 130.00 million Mt [6]. Spain, the United States of America and Bangladesh are some of the leading countries in poultry production, which, per annum, produce 7.70 million, 14 million and 4.25 million Mt respectively of PL waste [7]. In definition terms, Poultry Litter waste is an extract mixture of manure, chicken feathers, bedding material and spilled feed collected from the chicken breeding-slaughter houses and disposed of in landfills or open space as waste [8]. This waste is composed of high concentrations of inorganic elements (P, N, Ca, K, etc, 19 %, 14 %, 5.80 %, 2.50 % respectively), which, when improperly disposed of they result in environmental pollution problems [9]. For instance, application of the PL waste in agricultural farming as a fertilizer source leads to nutrient runoff into the waterways, resulting in excessive deposits of K and N causing eutrophication [10]. In addition, landfill disposal method emits ammonia and greenhouse gases (nitrous oxide and methane), which lead to global warming and poor air quality. On average, the global PL waste management emits 790 million Mt of CO_2e yr^{-1}, yet when managed, its carbon life cycle has the potential to be carbon neutral [11,12]. Bacteria like *Salmonella sp*. and viruses like Newcastle manifest and breed in the PL waste, which are transmitted and cause health issues to the animals and humans. The mentioned challenges that PL waste inflict on the environment and health result in an urgent need for a sustainable strategy in utilizing the resource as a beneficiation product.

One sustainable utilization method is using PL waste as a fuel source in combustion, which has a positive impact in reducing the demand for fossil fuels in energy generation, which helps in reducing the net carbon emissions and pollution. For example, the United Kingdom produces about 750 000 MWh of electricity from PL waste, which contributes to achieving a 120 CO_2kWh^{-1} of carbon intensity, that is significantly

lower than that of natural gas-fired power plants noted at 400 CO_2kW h^{-1} [13,14]. However, PL consists of high ash content (40 %), inorganic elements (Na, K, Cl, K, etc.), high moisture content (36 %) and low higher heating value (LHV) (8 – 12 MJ kg^{-1}), which, when directly combusted they slag, agglomerate, corrode and foul the combustion systems [15]. In addition, when combusted, they produce a low flame temperature and incomplete combustion, which emits high CO gases and particulates [16]. These poor physicochemical and thermal properties make the PL produce low thermal combustion efficiency, hence making it an undesirable feedstock for direct combustion application.

To mitigate these issues, PL is pretreated using demineralization methods such as mechanical particle size reduction and a distilled water leaching process. This reduces the ash content and inorganic elements in the PL, hence lowering the slagging, agglomeration and corrosion of the combustion systems. However, the demineralization process does not significantly improve the energy characteristics of the PL, such as higher heating value (HHV), low O/C and H/C ratio and energy density. Therefore, PL thermal and combustion properties are improved by thermally decomposing the waste in the absence of oxygen into biochar through the pyrolysis process [17]. Prior studies have retained 50.35 % biochar from pyrolysis reaction conditioned at 300 ℃ and 15 min with 4 mm particle size, attaining a higher heating value of 22.31 MJ $kg^{-1,}$ more than the HHV of raw PL (14.89 MJ kg^{-1}) [16]. The biochar produced from demineralized PL is more carbon dense (72 %), lower volatile matter (15 %), higher ignition temperature (300 ℃) and with improved combustion stability compared to the raw and demineralized PL [18]. Previous research [19,20] on biochar derived from PL has focused on soil amendments and fertilizer utilization, occupying a total global fraction of 70 %; yet, for energy application, 15 % of the global market focuses on that. Previous research has focused on characterizing biochar derived from PL, not from demineralized PL [21]. Also, the literature does not detail the biochar characterization on its candidacy as an alternative solid fuel, especially the one derived from the demineralization of PL [22]. Therefore, conducting the physiochemical, thermal, combustion, enthalpy and stoichiometric characteristics on the biochar derived from demineralized PL will add knowledge of the combustion performance of the fuel. In this study, the biochar derived from demineralized PL was evaluated against biochar from untreated PL for its physicochemical characterization. However, for thermal performance and combustion characteristics, the biochar from demineralized PL was studied at different heating rates to study its combustion stability and select a suitable combustion technology.

2. Experimental part

2.1. Poultry litter for Biochar production

PL samples composed of manure, wood shavings and sunflower husk were used in the production of biochar. The samples were collected from Tshipane farm and transported to the Botswana International University of Science and Technology biology laboratory, Botswana, where they were dried in an oven (Systronix Scientific, 278, South Africa) at 105 °C for 24 hrs and later grinded in a ball mill (Pulveisette 6, Fritsch, Germany) for 15 min to reduce the particle size [23]. The PL demineralization process was composed of a hybrid process of mechanical size fraction of 4 mm and deionized water (DI) leaching method (biomass-to-solvent ratio of 1:10 w/v, 2 hrs, 25 °C) [23]. The mentioned demineralization methods produced PL that had improved physicochemical, thermal and reduced inorganic elements in comparison to untreated PL prior to pyrolysis, as shown in Table 1.

Table 1 Physicochemical properties of untreated and demineralized PL [23]

Parameter	Untreated PL	Demineralized PL
Proximate analysis (%, db)		
Moisture content (MC_{ar})	9.74	5.34
Volatile matter	60.32	66.76
Fixed Carbon	17.61	19.74
Ash content	22.07	13.50
Ultimate analysis (%, db)		
Carbon	39.11	42.34
Hydrogen	5.2	4.28
Nitrogen	2.63	1.73
Sulphur	1.37	1.19
Oxygen	29.62	36.96
H/C ratio	1.59	1.21
O/C ratio	0.75	0.74
Lower Heating Value (MJ kg^{-1})	13.23	14.45
Higher Heating Value (MJ kg^{-1})	14.89	15.65

The demineralized PL was converted into biochar through the pyrolysis process shown in Figure 1. The pyrolysis reactor is made up of the following components: a vertical steel tube reactor, condensers, and incondensable gaseous holders. The demineralized poultry litter is inserted into the vertical steel tube reactor (ID: 0.06 m and H: 0.6 m), which is inserted into a muffled electrical furnace and sealed with a bolt and nut steel lid. Prior to pyrolysis, the pyrolysis reactor is flushed with nitrogen gas for 15 min at 103 kPa to create an inert environment.

The biochar production in this study adopted the low-temperature pyrolysis parameters occurring at the torrefaction–pyrolysis transition region mentioned by Nyoni and Kelebopile [16] of 300 °C for 15 min to produce biochar with 72 % energy yield [16]. The gases produced passed through the condensers (coolant set at 20 °C), and the condensable gases were converted into bio-oils while the incondensable gases settled into an incondensable gaseous holder.

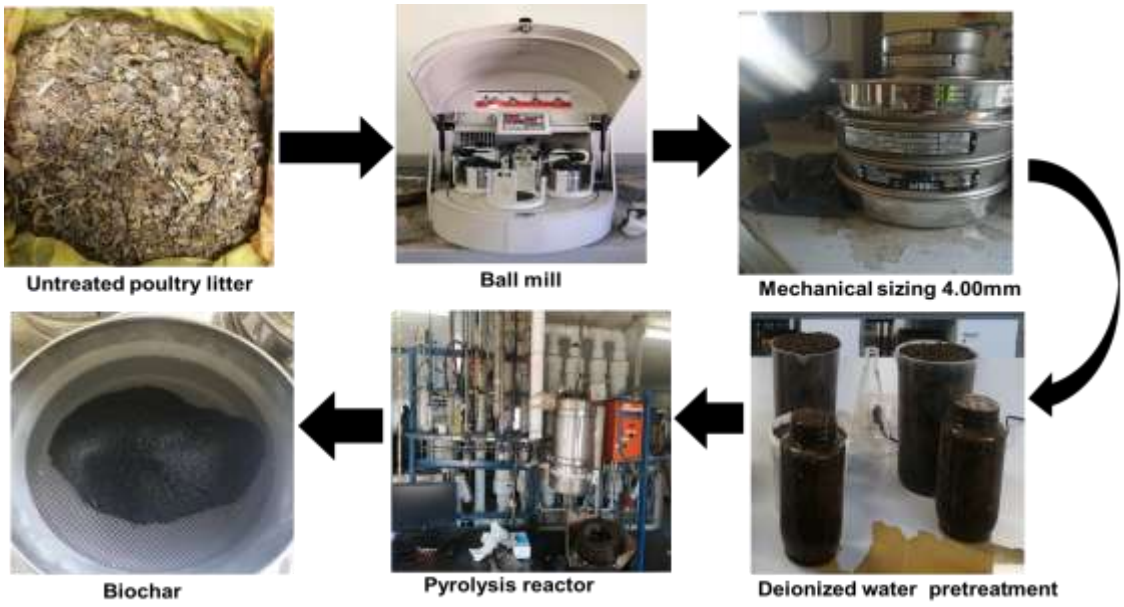

Fig. 1 Production of Biochar derived from demineralized PL through the low-temperature pyrolysis process

The solid residue left in the vertical steel tube after the reaction is the biochar. The biochar was collected, weighed and proceeded further for characterization to determine its properties.

2.2. Biochar characterization

2.2.1 Proximate analysis

Biochar's moisture, ash, volatiles and fixed carbon were analyzed by a thermogravimetric analyzer (TGA 701, Leco, USA) using the ASTM D1762 – 84 method [24]. Blank crucibles were inserted into the furnace carousel for baseline correction before inserting 1 – 2 g of biochar [25]. Moisture content was evaluated by heating the samples to 105 °C at a heating rate of 15 °C min^{-1} under a nitrogen flow rate of 15 L min^{-1} [26]. The temperature then increased to 700 °C at a heating rate of 50 °C min^{-1} under the same inert environment for the determination of the volatile matter content. The ash content was determined by heating the samples to 750 °C at 50 °C min^{-1} under an oxygen atmosphere. All measurements were determined on a dry basis (db) except for moisture content, which was determined as–received basis. Fixed carbon was obtained as shown in Equation 1:

$$FC(\%)=100-VM-AC \qquad (1)$$

where FC is Fixed Carbon, VM is Volatile matter, and AC is Ash content.

2.2.2 Ultimate analysis

Biochar's elemental composition (C, H, N and S) was analyzed by an elemental analyzer (Thermo Scientific Flash 2000 CHNS/O, USA) equipped with a thermal conductivity detector (TCD). ASTM D5373 – 16 (2021) method determined the C, H, and N, while the ASTM D4239 determined the S and the AC was determined using the ASTM D1762 – 84 [24]. Samples (1.75 – 1.85 mg) were weighed using a mass balance (Fisher brand CSC501, USA) and transferred manually into a sample run auto-injector, and the reaction was set at 950 °C under an oxygen atmosphere [27]. The Oxygen content was calculated by difference, shown in Equation 2, following the ASTM D3176 – 15(2020) method [28]. All parameters were measured on a dry basis (db).

$$O(\%)=100-(C+H+N+S+AC) \qquad (2)$$

2.2.3 Higher and Lower Heating Values

Biochar derived from demineralized PL Higher Heating Value (HHV_{db}) on a dry basis was determined by using the ASTM D5865-12 method [29]. Two grams of sample were weighed using a mass balance (Adam PGW438, USA), transferred into a ceramic crucible with the samples connected to the ignition wire using a cotton thread, and placed in a thermally insulated vessel containing a temperature transducer that records temperature change during the combustion process. The vessel was closed, filled with 3000 kPa pressure of oxygen, and combusted [30]. The heat generated is the higher heating value of the samples under study. In addition, the Lower Heating Value (LHV_{ar}) as received basis of the biochar was determined using Equation 3 [30].

$$LHV_{ar}=HHV_{db}(1-MC)-2.442(9H+MC) \qquad (3)$$

2.2.4 Thermogravimetric and differential thermogravimetric analysis (TGA and DTG)

Combustion properties of the biochar derived from demineralized PL were analyzed by a thermogravimetric differential analyzer (Mettler Toledo DSC/TGA 3+,

USA). Approximately 20 mg of the sample was weighed using a mass balance attached to the thermogravimetric differential analyzer and inserted into the furnace chamber. The combustion process was carried out in an air atmospheric condition with a flow rate of 100 ml min^{-1} and an operating temperature range of 25 – 1000 °C [31,32]. The experiments were conducted under four different heating rates (5, 10, 15 and 20 °C min^{-1}) for each sample [33]. Prior to inserting the weighed samples, a blank crucible was inserted into the furnace chamber to zero the weight of the crucible and act as a baseline correction. The TGA/DTG determined the combustion parameters, which are the ignition temperature (T_i), peak temperature (T_p), burnout temperature (T_b), maximum weight loss rate (DTG_{max}) and the average weight loss rate (DTG_{mean}) [34]. Ignition temperature is the temperature obtained when the sample losses 10 % of the initial mass, while burnout temperature is the temperature obtained at 95 % of the mass loss [35]. Peak temperature is the temperature that corresponds to the maximum weight loss of the sample. Thermal characterization of the demineralized biochar was conducted to determine critical properties required in the stoichiometric, enthalpy calculations, design and simulation of the combustion chamber.

2.2.5 Combustion performance indexes

The TGA/DTG combustion parameters stated in Section 2.2.4 were used to determine the combustion performance indexes of the biochar derived from demineralized PL. The performance indexes chosen are the ignition index (D_i), burnout index (D_b) and comprehensive performance index (D_c) derived from the TG/DTG temperature and reaction rates function as shown in Equations 4–6, respectively. The D_i shows how easy or hard the fuel is to ignite [32]. D_b reflects the rate at which the biochar burns, and a high D_b with a lower burnout temperature indicates a good burnout performance [25]. A high value of D_c shows that the fuel has a good combustion performance [36].

$$D_i = \frac{DTG_{max}}{T_i T_p} \qquad (4)$$

$$D_b = \frac{DTG_{max}}{T_b} \qquad (5)$$

$$D_c = \frac{DTG_{max} DTG_{mean}}{T_i^2 T_b} \qquad (6)$$

2.2.6 Kinetic analysis and thermodynamic analysis

The Kissinger model-free method uses the peak temperatures at maximum mass-loss rates derived from the TGA/DTG results at varying heating rates (5, 10, 15 and 20 °C min^{-1}) to determine the kinetic parameters under non-isothermal conditions. In contrast, mechanistic models like the Diffusion model or Random Pore model focus on the diffusional and physical aspects of combustion, like the oxygen reacting inside the fuel pores or on the surface at high temperatures. These mechanistic models are accurate when dominant mechanisms are known, but are less reliable when reactions involve multiple and overlapping pathways, like biochar. Kissinger's model-free method offers a broader application by not being constrained to a specific reaction mechanism [37]. This flexibility is best applied to apply on the biochar as the combustion reaction is in multiple-stage reaction. Hence Kissinger model-free method was selected to analyze the kinetics of the biochar derived from demineralized PL. The non-isothermal Kissinger model-free of first-order reaction (n=1) was used as it offers an effective kinetics description in determining the activation energy and Arrhenius constant of the biochar understudy. Equation 7 shows the Kissinger model-free model.

$$\ln\left(\frac{\beta}{T_p^2}\right) = \ln\left(\frac{AR}{E}\right) - \frac{E}{RT_p} \qquad (7)$$

where the X-Y plots are represented as follows: $\ln\left(\frac{\beta}{T_p^2}\right)$ is the y-axis, $\frac{1}{T_p^2}$ is the x-axis, $\frac{E}{R}$ is the gradient and $\ln\left(\frac{AR}{E}\right)$ is the y-intercept. The β is the heating rate (°C.min^{-1}), T_p is the peak temperature (°C), A is the Arrhenius constant or pre-exponential factor (min^{-1}), E is the activation energy (kJ mol^{-1}), R is the gas constant (kJ.$mol^{-1}K^{-1}$) [37]. Thermodynamic parameters, which are the Enthalpy change (ΔH), Gibbs free energy (ΔG) and Entropy change (ΔS), were determined using the following Equations 8-10, respectively.

$$H = E - RT \qquad (8)$$

$$G = E + RT\left(\frac{k_B T_P}{hA}\right) \qquad (9)$$

$$S = \frac{H - G}{T_P} \qquad (10)$$

where T is the absolute temperature (K), k_B is the Boltzmann constant (1.381×10^{-23} J K^{-1}), and h is the Planck Constant (6.626×10^{-34} Js).

2.2.7 Inorganic elements determination using X-ray Fluorescence (XRF)

Inorganic element composition in biochar contributes significantly to the corrosion, clinkering and slagging of the combustion systems through the lowering of the ash melting point, increase in ash deposits and reduced dew point temperatures [38]. A need to characterize the inorganic elements in the biochar derived from demineralized PL will determine the fuel indexes that will establish the suitability of the fuel for combustion and the selection of the best-suited combustion technology. A portable X-Ray fluorescence machine (Olympus Delta-50 Premium, USA; 4 W output) set at geochemist mode 50 kV and 10 kV configuration, each with 30 sec per configuration, was placed on top of a 2 cm

thickness sample to characterize the inorganic elements in the biochar understudy. The inorganic elemental composition was measured directly by XRF as elemental weight percentage (wt % of biochar) in the biochar. The measured inorganic elements were converted to oxide form using Equation 11 and normalized on a biochar inorganic ash basis (Equation 12), ensuring the cumulative normalized inorganic oxides sum to 100 % (Equation 13) [39].

$$W_{oxide} = XRF \times CF_{oxide} \quad (11)$$

$$W_{oxide,norm} = \frac{W_{oxide}}{W_{oxide,total}} \times 100\% \quad (12)$$

$$\sum W_{oxide,norm} = 100\% \quad (13)$$

where W_{oxide} is the oxide weight proportion (wt %), XRF is the inorganic elemental weight (wt %), CF_{oxide} is the oxide conversion factor adopted from James Cook University [39] conversion table, $W_{oxide,\ total}$ is the total oxide weight proportion, $W_{oxide,\ norm}$ is the normalized inorganic element oxides under the biochar inorganic ash basis (%).

2.2.8 Fuel indexes

The inorganic element compound oxides in the biochar ash determined using Equation 12, Sub-section 2.2.7, were used to determine the fuel indexes that contribute to the slagging, sintering and corrosion of the combustion chambers with the aim of determining the best-suited combustion technology [38,40]. The fuel indexes understudy were as follows: Base-to-acid ratio ($R_{b/a}$), Slagging/Babcock index (R_s), Silica to Aluminum ratio (Si/Al), Fouling index (Fu), Viscosity index (Sr), Alkali index/Mile index (Al, kg GJ^{-1}) and Bed agglomeration (BAI) expressed as Equations 14-20 respectively [40,41] were applied to the biochar produced from demineralized PL.

$$R_{b/a} = \frac{Fe_2O_3 + CaO + MgO + K_2O + Na_2O}{SiO_2 + TiO_2 + Al_2O_3} \quad (14)$$

$$R_s = R_{b/a} \times S \quad (15)$$

$$Si/Al = \frac{Si}{Al} \quad (16)$$

$$Fu = R_{b/a} \times (Na_2O + K_2O) \quad (17)$$

$$Sr = \frac{Si}{SiO_2 + Fe_2O_3 + CaO + MgO} \quad (18)$$

$$Al,\ kg\ GJ^{-1} = \frac{K_2O + Na_2O}{HHV} \quad (19)$$

$$BAI = \frac{Fe_2O_3}{K_2O + Na_2O} \quad (20)$$

2.3. Combustion chamber selection criteria

The selection of an appropriate combustion technology for biochar derived from demineralized PL is important to ensure efficient combustion and that optimal energy output is extracted from the fuel. The study investigated the suitability of the biochar understudy to combust in the following combustors: Grate chain (GFCC), Pulverized (PCC) or Fluidized bed (FBCC) combustion chamber, as each chamber has a specific fuel quality that it tolerates for effective combustion. The Pugh Decision matrix [42,43] was used to select the best combustion chamber that suits the biochar under study. The biochar quality was categorized under the following categories: Combustion efficiency, fuel handling, operational problems, frequency of maintenance, fuel reactivity and emissions potential and fouling and slagging [44]. The scoring was conducted on a scale of 1 to 5, where 1 represents poor suitability and 5 represents excellent suitability. Table 2 shows the decision matrix weight proportion selection of the biochar properties allocated to the above-mentioned categories.

The biochar's HHV properties were allocated a score of 5, as it has a significant effect on combustion efficiency [45]. The MC and AC were allocated a score of 4 as they assessed the fuel handling ability [44]. The R_s is given a score of 4 as it determines the ability of the biochar to cause operational problems [44]. The VM and FC have an indirect effect on combustion performance, and they affect the heating value; hence, they are allocated a score of 3 [45]. The H/C ratio and O/C ratio affect the fuel reactivity, and they are a contributor to the emissions; hence, they are allocated a score of 2 [46]. The $R_{b/a}$ indicates the fouling and slagging tendencies of biochar in the combustion chamber; hence, they were allocated a score of 2 [47]. The S and N were allocated a score of 1.67 as they affect pollution. The Al index was allocated a score of 1 as it provides additional data on the fouling and slagging. The score criterion is summed, and the total score is used to determine the proportion using Equation 21 [43]. The biochar fuel quality was evaluated in relation to the combustion chamber types' fuel quality tolerance range, and a weight score factor was established to show which combustion chamber was compatible with the biochar in the study. Equation 22 was used to determine the weight score used in the combustion chamber fuel compatibility ranking [48]. The rating allocated to each combustion chamber was based on how the specific properties of the biochar matched the specific tolerance of the chamber. The biochar parameters that were within the combustion chamber tolerance range were given a rating ranging from 4-5. Parameters near the chamber tolerance boundaries were rated between 2-3, whereas parameters exceeding the tolerance range were allocated a rating between 0-1.

$$Proportion = \frac{Score\ of\ a\ criterion}{Total\ score} \quad (21)$$

$$Weight\ Score = Proportion \times Rating \quad (22)$$

Table 2 Combustion chamber decision matrix weight proportion selection [44,49,50]

Criterion	Justification	Score	Proportion
HHV	Combustion efficiency	5	0.15
MC	Combustion efficiency and drying costs.	4	0.12
AC	Increases handling costs.	4	0.12
Rs	Critical for combustion operation.	4	0.12
VM	Affects combustion characteristics	3	0.09
FC	Contributes to the fuel's HHV	3	0.09
H/C ratio	Indicate fuel reactivity	2	0.06
O/C ratio	Indicate fuel reactivity	2	0.06
$R_{b/a}$	Indicate slagging and fouling tendencies.	2	0.06
S	Contributes to emissions	1.67	0.05
N	Contributes to emissions	1.67	0.05
Al, kg GJ^{-1}	Provides additional insight into slagging and fouling.	1	0.03
Total			1.00

2.4. Stoichiometric calculations of air and flue gas for demineralized biochar

The amount of air required to combust a kilogram (kg) of biochar fuel and the amount of flue gases produced were determined by calculating the stoichiometric. The stoichiometric calculations formulas used were adopted from Strecha [51], Vojtek [52] and Kitto & Stultz [53] previous studies that focused on combustion chamber designs. The biochar proximate analysis, ultimate analysis, and heating values data derived from Subsection 2.2 were applied to the calculations. All the volumes are referred to as minimum and expressed as normal cubic meters per kg of fuel (Nm^3kg^{-1} fuel) under standard state conditions (0 °C and 101.33 kPa). At 25 °C, the saturated vapor pressure and absolute pressure of humid air are 3.17 kPa and 99.59 kPa, respectively.

2.5. Enthalpy of air and flue gas

Components that constitute the flue gas (O_2, CO_2, N_2, H_2O, SO_2, Ar and ash) influence the enthalpy of flue gas when exposed to different temperatures. In addition, humidity in the air also affects the enthalpy of flue gas and air during combustion. The enthalpy of individual components that constitute flue gas, with their specific heat capacity at varying temperatures were used to determine the minimum enthalpy of flue gases per unit volume ($h^T_{FG,min}$), the specific heat capacity of humid air ($C^T_{P,ha}$), the enthalpy of humid air (h^T_{ha}), the enthalpy of fly ash (h^T_{FA}) and the enthalpy of flue gas (h^T_{FG}) from the combustion of 1kg of fuel. The minimum enthalpy of flue gases ($h^T_{FG,min}$) produced by the combustion of 1kg of fuel at α =1.00 at every specific temperature point (T).

2.6. Efficiency of the combustion chamber

Evaluation of the combustion chamber's thermal efficiency is critical in determining the performance of the system. The thermal efficiency was determined by evaluating the heat losses that the combustion chamber experiences during combustion. These heat losses are as follows:

- Heat loss in dry flue gases (L1).
- Heat loss due to hydrogen in the fuel (L2).
- Heat loss due to moisture in the fuel (L3).
- Heat loss due to moisture in the air (L4).
- Heat loss due to unburnt carbon (L5).

The Overall combustion efficiency (η_{cc}) was determined by subtracting all the heat losses (L1-L5) from 100 %.

3. Results and discussion

3.1. Biochar Physicochemical Characterization

Table 3 shows the findings on the physicochemical characteristics of the produced biochar from demineralized PL in comparison to biochar derived from untreated PL. The biochar understudy had undetectable MC compared to the one reported by Varanda et al. [54], which attained a 4.30 %. This shows that the drying process of the demineralized PL prior to pyrolysis was effective in moisture reduction compared to the other PL samples in the literature. A low MC in the biochar is desired as the combustion system will require less energy to evaporate the water, leading to an improved ignition, an increase in combustion temperature, and reduced fuel intake and air, leading to an overall improved combustion efficiency [55–57]. The VM of the biochar from demineralized PL (29.37 %) was in range with the one reported by Varanda et al., [54], slightly higher than the biochar from UT:PL and extremely lower than the ones reported by Kantarli et al., [58] which was 52 %.

Table 3: Physicochemical properties of biochar

Parameter	This Study	Biochar UT:PL	Kantarli et al., [70]	Varanda et al. [71]
MC_{ar}	0.00*	0.00*	-	4.3
VM	29.37	25.52	52.10	23.13
FC	52.00	43.76	-	43.19
AC	18.63	30.72	23.40	33.66
C	58.67	44.33	46.3	-
H	3.97	4.93	4.50	-
N	0.81	1.27	6.7	-
S	0.10	0.34	0.15	-
O	17.82	18.41	19.0	-
H/C ratio	0.81	1.33	1.16	-
O/C ratio	0.23	0.31	0.31	-
LHV (MJ Kg^{-1})	21.45	17.68	-	-
HHV (MJ Kg^{-1})	22.31	18.77	18.80	19.91

* undetectable, UT:PL is untreated poultry litter.

Lee et al. [59] noted that a good solid fuel for combustion should have VM in the range 20 – 40% so that it to ignite easily, hence having a steady reactivity. Therefore, our study biochar is within the recommended combustion VM range. However, the one reported in the mentioned literature above 50 % show an incomplete devolatilization at low temperature during pyrolysis, resulting in the produced biochar to be highly reactive, hence making it thermal unstable for storage, as it ignites unsteadily [58]. Hence, the demineralized biochar has high thermal stability, making it compatible with combustion as the fuel will produce fewer emissions and maximize energy retention [60].

Biochar prepared in this study had a high FC (52 %) compared to UT:PL biochar, which was similar to the one reported by Varanda et al. [54] FC (43.19 %). Demineralization improved the FC structure of the PL sample prior to pyrolysis, as evident from the demineralized PL (Table 1), which increased its FC from 17.61 – 19.74 % [55]. Additional, pyrolyzing the feedstock at high temperature (>300 ℃) resulted in high carbon retainment in the biochar structure, hence justifying the high FC in our study. The FC directly relates to HHV; hence, FC in demineralized biochar indicates high energy content in the fuel, which, when combusted, will produce high temperatures with long residence time [55].

Demineralized biochar in the study had a low AC of 18.63 % compared to the UT:PL biochar (30.72 %) and the one reported by Varanda et al. [54] (33.66 %). The biochar in-study, its PL was demineralized using DI and mechanical fractioning, resulting in the retention of ash in biomass particles with less than 1 mm and also dissolving the soluble salts, hence reducing the AC from 12.33 – 8.16 % (Table 1) prior to pyrolysis. The PL samples from UT:PL and Varanda et al. [54] were not demineralized, resulting in high AC retainment in their biochar [61]. However, Kantarli et al. [58] noted a low AC of 23.40 % the biochar despite the PL being undemineralized. This low in AC (23.40 %) might be caused by low temperature (250 ℃) being used during pyrolysis, which resulted in less organic matter being volatilized, hence a large fraction being retained in the biochar, resulting in AC being diluted in the biochar. The high AC in our study biochar, UT:PL biochar and the one reported by Varanda et al. [54] were produced under high temperature (>300 ℃) during pyrolysis, resulting in more organic structure being volatilized, hence AC being retained at high concentration in biochar. High AC is undesirable in the fuel intended to be used in combustion as this will contribute to the clinkering, corrosion and slagging of the combustion chamber while sinking the heat during combustion, thereby reducing the thermal efficiency [55].

A high C content in the demineralized biochar shows that the fuel is more stable thermally, possessing a high aromatic structure likely to have been influenced by the effective removal of inorganic elements in PL prior to pyrolysis and good, favorable pyrolysis conditions [62]. The S content was lower in the demineralized biochar (0.10 %) compared to the UT:PL biochar and Kantarli et al. [58]. During combustion, sulphur containing compounds emit toxic gases (H_2S and SO_x), which pollute the environment. The demineralized biochar has low S, meaning it has a reduced effect to become an S emission agent [63].

The N and H content in the demineralized biochar is lower than that of UT:PL biochar and the one reported by Kantarli et al. [58]. The reduction of N content promotes the demineralized biochar to be used as a fuel; when combusted, it will produce low NO_x emissions, thereby contributing to the reduction in greenhouse gases [64]. The decrease in H content in demineralized biochar (3.97 %) signifies that the fuel increased its C aromaticity as they correlated, promoting thermal stability and decreasing the devolatilization temperatures when combusted [65].

The O content is lower in the demineralized biochar (17.82 %) compared to UT:PL biochar (18.41 %). A lower O content is desired in fuel as it will have a high char reactivity and energy content due to the presence of low oxygenated functional groups in the structure [45]. Also, a lower O content corresponds to a lower O/C ratio, and the demineralized biochar O/C ratio is lower than the UT:PL biochar. A low O/C ratio shows that the fuel has a high degree of carbonization and is thermally stable, thereby promising to combust efficiently [58,66]. In comparison to the Kantarli et al. [58], the O/C ratio is within range. The demineralized biochar H/C ratio (0.81) is lower than the UT:PL biochar (1.33) and Kantarli et al. [58] (1.16). A lower H/C ratio increases the amount of aromaticity of demineralized biochar and shifts its carbonaceous material from raw PL to coal-like properties [67,68]. In addition, a low H/C ratio reduces the volatilization rate and tar formation during combustion, hence making the biochar release energy efficient and reducing char burnout time compared to UT:PL biochar. The

elemental composition of demineralized biochar shows that prior treatment of PL by reducing its inorganic elements improved the fuel's quality by increasing the C content and reducing the S and N content. This makes the fuel suitable for combustion as it offers a higher HHV with a low emissions effect.

The heating value of the demineralized biochar (LHV_{ar} and HHV_{db}, 21.45 and 22.31 MJ $kg^{-1,}$ respectively) was high compared to the UT:PL biochar (LHV and HHV at 17.68 and 18.77 MJ $kg^{-1,}$ respectively) and literature, which was of undemineralized biochar (HHV: 18.80 MJ kg^{-1} [58] and 19.91 MJ kg^{-1} [54]). This reflects the relevance of demineralization of PL prior to pyrolysis in energy retention in the biochar, as the biochar in the study improved its energy content. The elemental C content of demineralized biochar (58.67 %) was 14.35 % points and 12.37 % points higher than that of UT:PL biochar and the one reported by Kantarli et al. [58]. This high value of C content in demineralized biochar is corroborated by its corresponding HHV_{db} [68,69].

3.2. Thermogravimetric analysis of demineralized biochar

The results for the thermogravimetric and differential thermogravimetric (TGA/DTG) of biochar derived from demineralized PL are presented in Figure 2 and Table 4 under varying heating rates (5, 10, 15 and 20 °C min^{-1}). The TGA/DTG results investigate the thermal stability, degradation behavior and combustion performance of the demineralized biochar. TGA curves in Figure 2a, summarized temperature points in Table 4, show the combustion process of demineralized biochar going through a multi-step decomposition process at all varying heating rates (5, 10, 15 and 20 °C min^{-1}). The loss of moisture is observed in a temperature range between 58.70 – 92.44 °C at the four varying heating rates. A negligible peak was observed for the evaporation of moisture, as it constitutes the MC constitutes a mass fraction of 3.64 % (Table 3, Sub-Section 3.1). An increase in heating rate (β) increased the shift of the evaporation temperature. Peak temperatures 1 and 2 signified the devolatilization and char combustion stages, respectively, of the biochar, noting the presence of lignocellulosic in the biochar [70]. An increase in heating rates results in two distinct trends to be observed. A significant weight loss is observed at higher temperatures; for instance, biochar at a lower heating rate (5 °C min^{-1}) releases volatiles and main decomposition in a stepwise approach at lower temperatures compared to a higher heating rate (20 °C min^{-1}), which release volatiles and main decomposition at high temperatures due to less available time to conduct a sufficient heat transfer and molecular rearrangement per each temperature increment. Other researchers [70,71] also noted the same thermal behavior of biochar, which is that higher heating rates reduce the reaction time of molecule structures, which react at lower temperatures, shifting them to higher temperatures where they decompose at a larger mass fraction. The DTG curves shown in Figure 2b show the combustion stages of the demineralized biochar through the identification of temperature-dependent reactions. In addition, Table 4 summarizes the key values from the TGA/DTG graphs (Figure 2).

The maximum DTG peaks show a temperature point where the mass loss rate is at its maximum. This peak point influences the combustion reactivity, which is determined by the heating rate and biochar intrinsic properties [49].

Table 4 TGA/DTG of the biochar

Heating rate (°C min-1)	Reaction region (°C)	Temperature (°C) 1	2	DTGmax
5	58.57-476.00	388.58	440.93	-0.011
10	92.44-487.03	416.45	444.88	-0.017
15	91.24-527.10	394.65	455.93	-0.029
20	85.00-548.93		415.47	-0.027

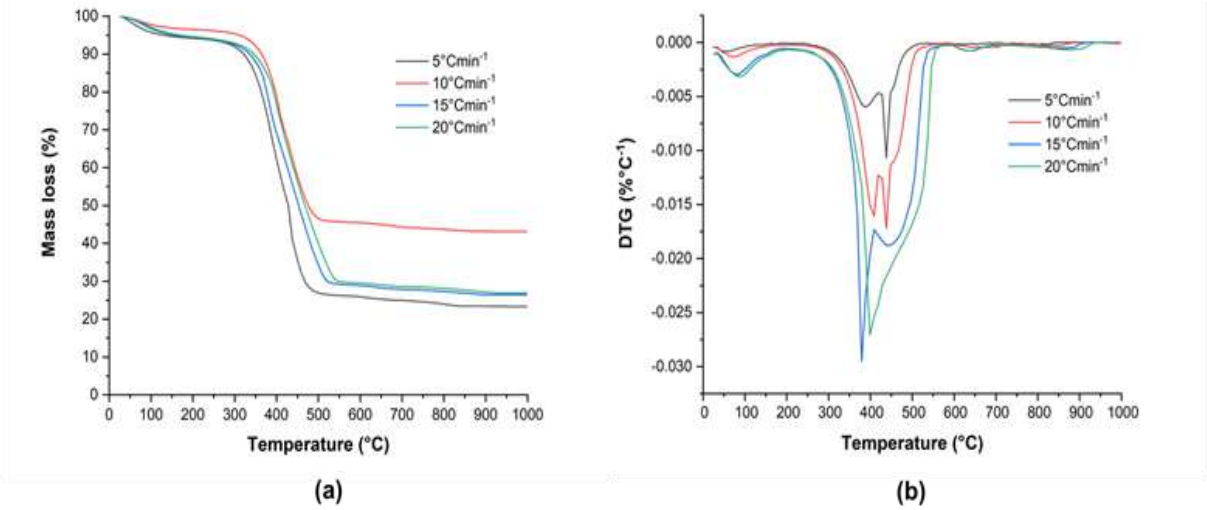

Fig. 2 Biochar derived from demineralized poultry litter at different heating rates (5, 10, 15, and 20 °C min^{-1}) (a) TG curves (b) DTG curves

At lower heating rates (5 and 10 °C min^{-1}), a stepwise degradation pattern is observed, but at higher temperatures (388.58–416.45 °C) and which signifies the presence of heavy hydrocarbons as noted with the high FC. In addition, the maximum DTG happens at peak 1 temperatures, showing that the biochar is less reactive at these heating rates (5 and 10 °C min^{-1}). The lower heating rate is applicable in combustion systems that require lower peak temperatures or controlled burn rates [70]. As the heating rate increases (15 and 20 °C min^{-1}), the reaction shifts towards the higher temperatures (Table 4), with peak DTG happening at a temperature range of 395 – 415 °C. This shows that higher heating rates result in a bulk of biochar composition, including the volatiles being released at higher temperatures, leading to localized overheating in the combustion systems and altering the pollutant formation dynamics [72]. Also, higher heating rates make the biochar hard to ignite and volatilize with reduced heat distribution during combustion [25]. Higher heating rates produce a shaper and more intense combustion at higher temperatures, making it favorable for energy production. This affects the combustion chamber design, ignition strategy, and residence times of biochar combustion [73].

Peak temperatures for 5 and 10 °C min^{-1} were observed in the thermal degradation stage at higher temperatures compared to the 15 and 20 °C min$^{-1,}$ which happened in the combustion devolatilization stage. This shows that the thermal decomposition kinetics and combustion reactivity of biochar derived from demineralized PL are significantly influenced by the heating rates. The biochar in the study had high FC compared to VM, which is why much of the mass loss and peak temperature occurred in the char combustion stage. An increase in heating rate will result in fewer peaks formed, as shown on the heating rate of 20 °C min^{-1} sample, which signified a concurrent combustion of VM and char at high temperatures [74].

3.3. Combustion characteristics and reactivity indexes

Figure 3 shows the combustion characteristic for the biochar derived from demineralized PL at varying heating rates (5, 10, 15 and 20 °C min^{-1}). The ignition temperature (T_i), burnout temperature (T_b), ignition index (D_i), burnout index (D_b) and comprehensive performance (D_c) are the characteristics presented in Figure 3a-d, respectively. An increase in heating rate from 5 to 20 °C min^{-1} results in an increase in temperatures for both the ignition (T_i) and burnout (T_b) (Figure 3a).

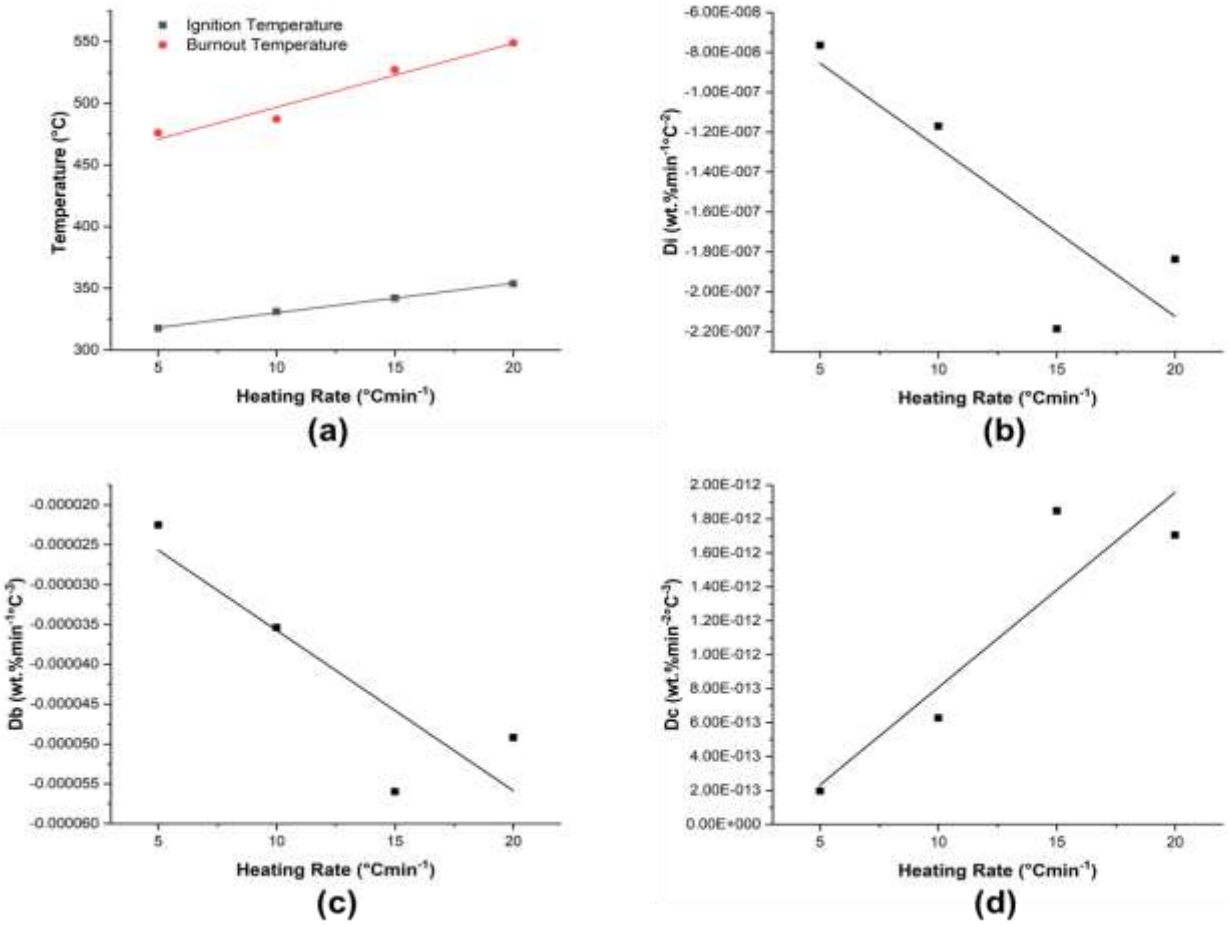

Fig. 3 Combustion characteriochar derived from poultry litter at four heating rates (5, 10, 15 and 20 °C min^{-1}) (a) ignition and burnout temperatures, (b) ignition index, (c) burnout index, (d) comprehensive performance

Lower heating rates promote prolonged heating of the biochar at sub-pyrolytic temperatures, resulting in a gradual release of volatiles and partial oxidation, hence making ignition happen at low temperatures compared to high heating rate conditions [75]. Our findings agree with other authors [70,71], who noted a shift in critical reaction steps to higher temperature regions when biochar was reacted at a higher heating rate. Higher heating rates result in a reduced reaction time at each intermediate temperature, making the biochar hard to ignite and less volatile [76]. Burnout temperature performed the same trend as the ignition temperature with the change in heating rate. At low heating rates (5 and 10 °C min^{-1}), the biochar organic structure combusts steadily and achieves complete combustion at lower temperatures. In contrast, high heating rates delay the onset of combustion of the char organic structure in the biochar, shifting the critical combustion reactions to higher temperature intervals, hence raising the burnout temperature [21]. The ignition and burnout temperatures under varying heating rates are important in combustion chamber operational optimization and mitigating the fouling and slagging effects [34].

Combustion reactivity and performance can be analyzed quantitively using indexes like the ignition index (D_i), burnout index (D_b) and the comprehensive index (D_c). Figures 3b and c show the D_i and D_b of biochar derived from demineralized PL under varying heating rates (5, 10, 15 and 20 °C min^{-1}). The D_i assesses the promptness and ease of ignition, while the D_b measures the efficiency and completeness of char combustion. As shown in Figures 3b and c, the heating rate results are inversely proportional to the D_i and D_b. At a low heating rate (5 °C min^{-1}), the Di is higher compared to a high heating rate (20 °C min^{-1}). This shows that a low heating rate promotes steady volatilization and oxygen infiltration, making biochar ignite easily [73].

Also, at lower heating rates (5 and 10 °C min^{-1}), the burnout index (D_b) has high values compared to higher heating rates (15 and 20 °C min^{-1}). At a lower heating rate, the biochar is exposed to a prolonged time under moderate temperatures, which gives enough time for the char to be oxidized thoroughly, achieving a complete burnout at comparatively lower temperatures [72]. An increase in the heating rate results in a decrease in both the D_i and D_b indexes, showing a shift towards difficult ignition conditions and less efficient burnout conditions. A high heating rate results in the biochar heating through crucial temperature ranges quickly, resulting in insufficient time for the molecules to break chemical bonds, absorb energy and form new intermediate or radical species [77]. This causes the decomposition to shift to higher temperatures where there is enough thermal energy for the reactions to occur rapidly, resulting in ignition delay and a shift of critical combustion stages towards high temperatures [78]. In addition, a higher heating rate during combustion makes the volatiles not have enough time for the production of reactive radicals, oxygen mixing and exothermic reactions, making it challenging to achieve a stable flame in the short time available, making it hard to sustain the reaction to completion [70].

In contrast, the comprehensive performance index (D_c) (Figure 3d) has a positive correlation with the heating rate. A high D_c at higher heating rates is due to the rapid and intensified combustion dynamics once the ignition is attained [36]. Although ignition and burnout conditions become more demanding, the overall integrated performance may improve due to faster volatile release and subsequent char oxidation within a narrower and more energetically dense temperature regime [71]. Such behavior suggests that under certain controlled conditions, higher heating rates can lead to a more concentrated and potentially higher energy-yielding combustion profile despite less favorable ignition and burnout indexes individually [75]. For industrial applications, if the biochar is to be used under a low heating rate, it is best applicable to systems that target controlling the burning rate or achieving stable flame fronts or fixed-bed combustion chambers. In contrast, for high heating rates, flash combustion chambers or entrained flow chambers will be best applicable as they will benefit from the higher D_c index at the expense of higher T_i and T_b. The influence of heating rate on the combustion characteristics and reactivity indexes gives a detailed understanding of the biochar thermal and combustion responses that will guide the design of a combustion chamber.

3.4. Kinetic and thermodynamic analysis

Kissinger plot shown in Figure 4 extracted the kinetics parameters from non-isothermal thermogravimetric (TGA) data in the combustion process.

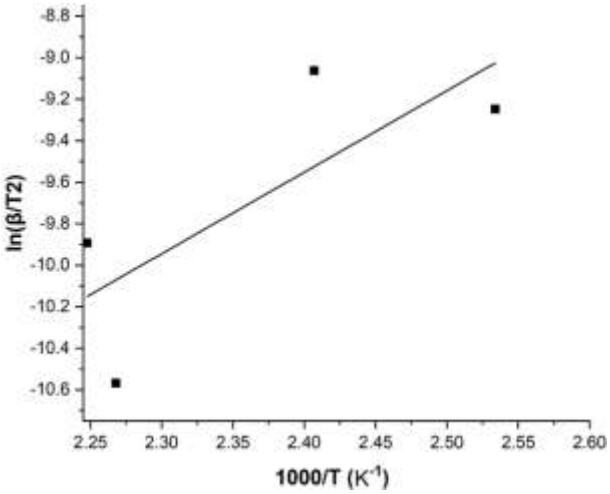

Fig 4 Kissinger plots for the main mass loss of the biochar derived from demineralized PL

These kinetic parameters are the activation energy (E_a) and Arrhenius constant (A) as shown in Table 5. The E_a is 32.75 kJ mol^{-1} for the biochar derived from demineralized PL. Literature notes that E_a for biochar derived from pyrolyzed biomasses ranges between 30-200 kJ mol^{-1} [79,80].

Table 5 Thermodynamic parameters for biochar derived from demineralized PL

Parameter	Value
E_a (kJ mol^{-1})	32.75
A (min^{-1})	6.91×10^{11}
ΔH (kJ mol^{-1})	35.02
ΔG (kJ mol^{-1})	80.49
ΔS (kJ mol^{-1})	-0.065

Our findings show that the biochar in the study is at the lower end of the E_a spectrum in comparison with the literature, signifying the low energy required for the biochar to initiate ignition, thus exhibiting a more rapid, facile thermal decomposition [81]. The low E_a in the biochar derived from demineralized PL can be attributed to the presence of a low content of inorganic elements that would alter the combustion pathways. In undemineralized PL biochar, the presence of these inorganic elements in large quantities catalyzes specific thermal degradations, thereby increasing the overall E_a [82]. Upon demineralization, these inorganic elements are largely removed, moving the dominant decomposition mechanism to lower energy routes [83].

Arrhenius constant shows the rate at which biochar particles collide with each other, surpassing their energy barrier, and a value range of $10^{11} – 10^{13}$ min^{-1} signifies a high Arrhenius constant of biochar derived from pyrolysis [71]. Our study has a high Arrhenius constant of 6.91×10^{11} min^{-1}, which indicates a relatively facile reaction once the E_a threshold is met, which is consistent with the presence of highly reactive organic fractions within the biochar matrix [25]. Under the combustion environment, a lower E_a (32.75 kJ mol^{-1}) shows that the biochar is ignited at mild temperatures with a rapid mass loss once ignition is initiated. This makes the biochar in the study ideal for application as a fuel, as it ignites faster and burns completely, provided that sufficient oxygen is supplied [84]. However, a high Arrhenius constant (6.91×10^{11} min^{-1}) of the biochar signifies the ability of the fuel to create hotspots or partial oxidation that escalates the reaction rate in the combustion chamber [85].

Table 5 shows the thermodynamic parameters, which are the enthalpy change (ΔH), Gibbs free energy (ΔG) and the entropy change (ΔS) for the biochar derived from demineralized PL. The difference between E_a and H (32.75 – 35.02 kJ mol^{-1}) is -2.27 kJ mol$^{-1,}$ which is negligible. Such a negligible difference between E_a and H signifies that the cleavage of weak bonds dominates the main pyrolysis and oxidative reaction processes, mostly the C–C linkages and predominantly C–O bonds. A high positive Gibbs free energy (80.49 kJ mol^{-1}) was noted on the biochar in the study, signifying a need for external thermal energy for the biochar to initiate any thermal reaction [82]. The demineralized biochar entropy change was -0.065 kJ mol$^{-1,}$ which indicated stable gaseous products production than the reactants, hence producing a more exothermic reaction during combustion [71].

3.5. Inorganic element composition

Biochar comprises inorganic elements made up of metal (K, Ca, Al, Mn, Fe, Cr, Cu, Zn, Rb, Sr, Y, Zr, Nb, Mo, Ba) and non-metal (P, S, Si, Cl) elements present in different compositions as shown in Figure 5. These inorganic elements comprise most of the fuel ash fraction. When combusted, the fuel's inorganic elements are separated, evaporated, precipitated, nucleated and coagulated to form ash particles that are either acidic or basic compounds [86]. These ash particles contribute to the slagging, corrosion and agglomeration of combustion chambers [60]. The inorganic elements in the fuel were further categorized based on their volatility. K, S and Cl are the most volatile elements, with K constituting the highest fraction of 7 %, while others were less than 1 %. Mn and P elements are semi-volatile, with P constituting the highest non-metal element fraction of 1.18 %. Al, Ca, Fe and Si aref non-volatile elements, with Ca and Si constituting the highest fraction in their metal and non-metal categories, respectively. Cr, Cu, Zn, Rb, Sr, Y, Zr, Nb, Mo, and Ba are minor heavy metals (<1 %), and when combusted, they react with Cl, causing a reduction in ash melting point and heavy metal emissions.

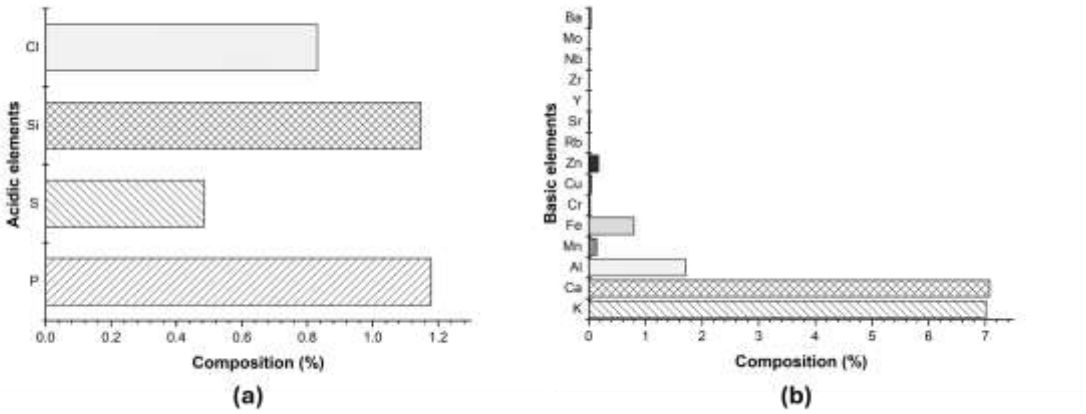

Fig. 5 Biochar inorganic elemental composition measured by XRF (wt % of biochar) (a) acidic elements, (b) basic elements

This contributes to the corrosion and agglomeration of combustion chambers. The biochar's inorganic elements, when combusted, undergo a primary ash transformation reaction where the inorganic elements have a high oxygen affinity in relation to the oxygen affinity of the fuel's C–H matrix. The inorganic elements' ash transformation reactions will form acidic and basic compounds (Figure 6a) that vary with their reactivity (Figure 6b).

The reactivity order of the ash transformation reactions is based on the element's thermodynamics and effect on temperature [87]. Non-metal elements, when combusted, form acidic compounds that have a negative effect on the combustion chamber system. The P element is highly reactive compared to the other non-metal elements and when combusted, it reacts to form a P_2O_5 compound, which has the highest non-metal oxide (9.11 %) in the study. The P_2O_5 can react with other ash components, forming low-melting point compounds that can lead to slagging and fouling in the combustion chambers, hence reducing combustion efficiency and increasing maintenance costs [38]. The S element is highly volatile compared to Si and Cl elements, as shown in Figure 5. During combustion, the S element tends to have a lower affinity to O_2 compared to the C–H biochar fuel matrix; hence, it will react with the fuel matrix to form H_2S(s) and S_2(g) that will further react with O_2 to form SO_x(g) emissions (SO_2 and SO_3). The SO_3 emissions corrode the combustion chambers; therefore, the concentration of the SO_3 should be low, as shown in the biochar understudy, resulting in the lowest composition at 4.08 %. The Si element is in amorphous form ($SiO_2.H_2O$); when combusted, it produces small silica particles (SiO_2) that agglomerate in the combustion chamber, being one of the high non-metal oxides at 8.27 %. Cl element exists as weak acids in the biochar fuel, and when combusted, it produces Cl_2(g), which further reacts with the fuel's moisture to form a toxic compound containing HCl(g) acids. The HCl formed compound will lower the ash melting point, which forms furans and dioxins while increasing the corrosion effect on the combustion chambers. In addition, this compound has a low volatility, hence making a significant fraction of the ash. The biochar understudy has an insignificant fraction of the Cl element (<1 %), making it less likely to have a significant negative effect on the combustion chamber.

The metal elements form basic compounds when combusted. The K_2O oxide is high (28.50 %), increasing the susceptible chance of aerosol formation during combustion. In addition, the volatile KOH is formed, reducing the ash melting temperatures and corroding the combustion unit systems. The CaO constituted a high fraction (33.39 %), resulting in an increased chance of aerosol formation during combustion. These aerosol particles will be deposited in the combustion chamber. Al_2O_3 had a significant oxide composition (10.87 %); due to its high melting point, it acts as a heat absorber, thereby reducing the combustion temperature [88]. In addition, Al_2O_3 can react with other ash components, potentially affecting their melting point, sintering behavior, and potential for slagging or fouling in the combustion chamber. Also, it acts as a catalyst for faster combustion while reducing emissions by capturing NO_X and SOx. Fe_2O_3 and MnO constitute a low fraction (3.86 % and 0.61 %, respectively) and when combusted, they do not affect the combustion unit systems due to their non-reactivity with ash-forming elements and are retained in ash. Heavy metal oxides (Cr_2O_3, ZnO, Rb_2O, SrO, Y_2O_3, ZrO_2, MoO_3 and BaO) were insignificant (<1.10 %); hence, they did not participate in the combustion process but rather acted as heat-absorbing compounds [40]. This means that the fuel can be applied in small combustion systems without electrostatic precipitators [60].

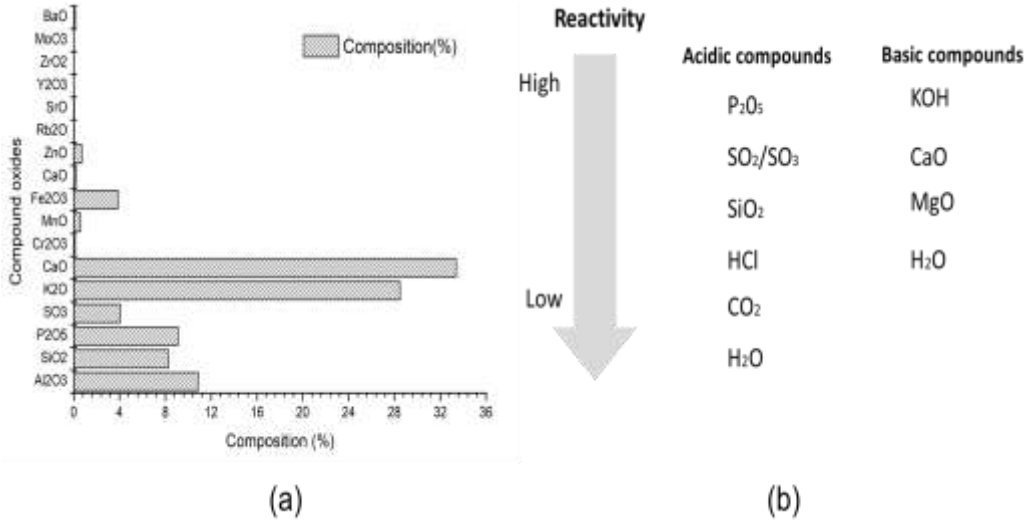

Fig. 6 Normalized oxide composition of the biochar inorganic ash composition derived from XRF (a) Composition (b) Reactivity

3.6. Fuel index analysis

The slagging and fouling behavior of the fuel under study has been analyzed, as shown in Table 6. The base-to-acid ratio ($R_{b/a}$) is very high at 3.43>1.75, indicating a high slagging tendency with a low ash melting point of the fuel when combusted in the combustion chamber [89]. In addition, the Slagging/Babcock index (R_s, 1.67) does support that the fuel has a high slagging behavior, with sulfur contributing significantly to the alkali sulfate deposits that are unstable during combustion [90]. The silica-to-aluminum ratio (S/A) reflects the relative proportions of two key ash components that significantly influence melting behavior and slagging risk [61]. A high silica content increases the melting point and slagging risk, while Alumina contributes less significantly. A low ratio of S/A (0.67) signifies a low risk of ash melting. The Fouling index (Fu) is 97.89, which indicates a high potential risk of slagging, fouling, and corrosion if combusted in the traditional combustion chambers [74]. The slagging ratio (Sr) is low at 0.03, which causes unease flow of molten ash, resulting in a high risk of slagging, fouling and corrosion of the combustion chamber [91]. The Alkali index (Al, kg GJ^{-1}) of the fuel signifies a moderate slagging of the ash on the combustion chamber walls or convection surfaces exposed to the radiant heat [38]. The fuel under study has a Bed agglomeration (BAI) of 0.14, making the agglomerates impede the contact of fuel with air, resulting in incomplete combustion. In addition, high agglomerate has a high risk of depositing on the combustion chamber walls, resulting in slagging and fouling.

3.7. Combustion chamber selection

A critical analysis of the biochar properties in relation to the combustion chamber fuel tolerance specification helps in selecting the combustion chamber that best suits the fuel in the study. Table 7 shows a comparative analysis of biochar properties against combustion chamber fuel tolerance specification, mainly for the Grate-fired combustion chamber (GFCC), Pulverized combustion chamber (PCC) and Fluidized combustion chamber (FBCC). The demineralized PL biochar's HHV of 22.31 MJ kg^{-1} is above the minimum threshold for PCC and within range for the GFCC and the FBCC. The biochar's HHV value shows that the fuel can efficiently be converted to heat without straining all three chambers. The biochar's VM (29.37 %) is compatible with GFCC, PCC and FBCC, while the FC (52 %) is slightly above the GFCC tolerance but in range with the rest of the combustors. A high FC will ensure that high-energy-density fuel is supplied to the chamber while providing stable combustion [30]

Table 6 Fuel indexes of biochar derived from demineralized PL fuel index in comparison with the slagging scale

Indexes	This Study	Slagging range [86,89,92]			
		Low	Medium	High	Very high
$R_{b/a}$	3.43	<0.50	0.5 – 1.00	1.0 – 1.75	>1.75
R_s	1.67	<0.70	0.7 – 1.00	1.0 – 1.30	>1.30
Si/A	0.67	<1.87	1.87 – 2.65	>2.65	-
Fu	97.89	<50.00	50 – 100.00	>100.00	
Sr	0.03	>72.00	65 – 72.00	<65.00	-
Al, $kgGJ^{-1}$	1.26	<0.17	0.17 – 0.34	>0.34	-
BAI	0.14		-	<0.15	-

Table 7 Combustion chamber technology specification sheet in comparison with parameters of the studied biochar

Parameter	Biochar	Combustion chamber [54,108]		
		GFCC	PCC	FBCC
MC (%)	0.00*	<50.00	<15.00	<60.00
VM (%)	29.37	10 – 70.00	15 – 45.00	10 – 80.00
FC (%)	52.00	10 – 50.00	30 – 55.00	10 – 50.00
AC (%)	18.63	<30.00	<5.00	Up to ~50.00
N (%)	0.81	<2.00	<3.00	<3.00
S (%)	0.10	<2.00	<4.00	<6.00
H/C ratio	0.81	<1.20	<1.00	<1.30
O/C ratio	0.23	0.20 – 0.70	0.10 – 0.30	0.20 – 0.70
HHV (MJ Kg^{-1})	22.31	8.00 – 25.00	>15.00	5 – 30.00
$R_{b/a}$	3.43	<0.70	<0.50	>1.00
R_s	1.67	<1.00	<2.00	0.5-2.50
Si/Al	0.67	0.5 – 1.50	0.5 – 1.50	0.3 – 20.00
Al (kg GJ^{-1})	1.26	<0.50	<0.17	0.6-1.50

The fuel's MC was undetectable and in the tolerance range of all the combustors in the study. The demineralized biochar AC (18.63 %) was high for the PCC and in range for the GFCC and FBCC. It is important to manage the AC in the GFCC and PCC carefully to avoid fouling and slagging. The FBCC's ability to effectively mix the reactants and distribute heat efficiently tolerates high AC [93]. The H/C and O/C ratios of the biochar are within the tolerance range for the GFCC, PCC and FBCC. The PCC tolerates a low O/C ratio to ensure efficient combustion with low CO emissions. However, our biochar has an O/C ratio near the high tolerance range of the PCC, hence an optimized operation will be recommended to ensure an efficient combustion with low CO emissions [45]. Performance indexes like $R_{b/a}$, Rs and S/A favor the FBCC chamber due to its fluidization ability to accommodate fuel with a high surface ratio and bulk density that promotes enhanced reaction kinetics. The Al (kg GJ^{-1}) index exceeded the GFCC and PCC, making the FBCC the preferred combustion chamber in terms of tolerance to fouling and slagging. The S and N content were in the emission tolerance range on all the combustion chambers, although a need to control NO_X emissions in the PCC operations is relevant [94].

The Pugh Decision matrix shown in Table 8 was used to select the most preferred combustion chamber quantitatively. The weight scores were allocated to each chamber type based on the literature. The FBCC was the first preferred combustion chamber of choice to combust the biochar, as it had the highest score of 5. The GFCC and PCC were a dual second preference, both with an equivalent score of 3.89.

3.8. Stoichiometric calculations for demineralized biochar

3.8.1 Theoretical amount of air required for the combustion of demineralized biochar

Table 9 shows the stoichiometric calculation results of the amount of air required to combust a kilogram of biochar fuel. Studies [95,96] recommend an equivalence ratio (ϕ) of 0.80 for the FBCC, which corresponds to an excess air of 25 % to combust the biochar to completion.

Table 8 Pugh Decision matrix on the type of combustion chamber technology

Parameter	Proportion	GFCC		PCC		FBCC	
		Rating	Weight Score	Rating	Weight Score	Rating	Weight Score
HHV	0.15	5	0.75	5	0.75	5	0.75
MC	0.12	5	0.60	5	0.60	5	0.60
AC	0.12	5	0.60	0	0.00	5	0.60
R_s	0.12	0	0.00	4	0.48	5	0.60
VM	0.09	5	0.45	5	0.45	5	0.45
FC	0.09	4	0.36	5	0.45	5	0.45
H/C ratio	0.06	5	0.30	5	0.30	5	0.30
O/C ratio	0.06	5	0.30	5	0.30	5	0.30
$R_{b/a}$	0.06	0	0.00	0	0.00	5	0.30
N	0.05	5	0.25	5	0.25	5	0.25
S	0.05	5	0.25	5	0.25	5	0.25
Al (kg GJ^{-1})	0.03	1	0.03	2	0.06	5	0.15
Total	1.00		3.89		3.89		5
Rank			2		2		**1**
Continue			No		No		**Yes**

Table 9 Stoichiometric calculation of air required to combust a kilogram of biochar

Parameter	Symbol	Amount
Excess air @ ϕ of 0.80	α	25 %
Minimum volume of oxygen to burn 1kg of fuel	$V_{O2,min}$	1.072 $Nm^3\ kg^{-1}$ fuel
Minimum volume of dry air	$V_{DA,min}$	5.104 $Nm^3\ kg^{-1}$ fuel
Water vapor at 1m3 of dry air	VH_2O	0.023 $Nm^3\ kg^{-1}$ fuel
Air correction factor	f_{corr}	1.023
Minimum volume of humid air	$V_{RH,min}$	5.220 $Nm^3\ kg^{-1}$ fuel
Actual volume of air used to combust a unit of biochar fuel	$V_{A,act}$	6.525 $Nm^3\ kg^{-1}$ fuel
Actual mass of air used to combust a unit of biochar fuel	$m_{A,Act}$	7.830 kg kg^{-1} fuel

Hence, this work used 25 % excess air in its combustion process to ensure stable fluidization is maintained while effectively mixing the reactants and reducing the unburnt carbon [44,97]. Our findings are consistent with prior research [44,98,99], which noted that the use of moderate excess air supply ranging between 20 – 30 % in the FBCC improves the combustion efficiency while ensuring that low NO_x emissions are maintained in the combustion process.

The calculations of the stoichiometric show that the minimum volume of oxygen (V_{O2min}) required to combust 1kg of biochar fuel completely was 1.072 $Nm^3\ kg^{-1}$ fuel. Balazi [100] noted that the V_{O2min} a kg of fuel ranged from 0.851 – 1.258 $Nm^3\ kg^{-1}$ fuel for wood to coal fuels. Hence, our biochar transitioned from biomass properties to coal structure, and its V_{O2min} is within the range for a biochar, coal-like fuel. The minimum volume of dry air ($V_{DA,min}$) required to supply the required oxygen for complete combustion was 5.104 $Nm^3\ kg^{-1}$ fuel. Our findings were in agreement with the literature [44,101] for $V_{DA,min}$ range of 4.500-5.500 $Nm^3\ kg^{-1}$ fuel for biomass and biochar fuels to achieve a complete stoichiometric combustion. Dry air consists primarily of N_2 and O_2 at 79 % v/v and 21 % v/v, respectively [100].During combustion, the N_2 acts as a heat sink, assisting by controlling the flame temperature, thereby reducing the risk of thermal NO_x formation, a common pollutant in high-temperature combustion processes [51]. The water vapor content in air (V_{H2O}) used for combustion was 0.023 $Nm^3\ kg^{-1}$ fuel, which is almost in comparison to the absolute humidity (0.015 Nm^3 H_2O vapor m^{-3} air at 25 ℃) [99]. The V_{H2O} in the study has no effect on the flame temperature and stability during combustion [102]. The $V_{RH,\ min}$ was 5.220 $Nm^3\ kg^{-1}$ fuel, showing that air added 0.116 $Nm^3\ kg^{-1}$ fuel of moisture ($V_{RH,min} - V_{DA,min}$) into the combustion. The actual volume of air ($V_{A,act}$) required for combustion was 6.525 $Nm^3\ kg^{-1}$ fuel and the actual mass of air ($m_{A,Act}$) was 7.830 kg kg^{-1} fuel, corresponding to reports from Balazi [100].

3.8.2 Theoretical amount of flue gas produced by the combustion of demineralized biochar

The amount of flue gas produced during the combustion of 1kg of demineralized biochar is shown in Table 10. During the combustion of a kilogram of demineralized biochar, the following volumes of flue gases were produced: V_{CO2}, V_{SO2}, V_{N2}, V_{Ar} and $V_{DFG,min}$ 1.209, 0.003, 4.007, 0.047 and 5.226 $Nm^3\ kg^{-1}$ fuel, respectively. The demineralize biochar constitutes 56.95 % of elemental C in its biochar structure, hence the CO_2 flue gas constitutes the main output gas. The V_{SO2} produced by biochar is relatively small, meaning that the fuel is insignificant in making SO_x emissions that contribute to acid rain and respiratory issues. Literature notes that the V_{SO2} ranges between 0.002 – 0.005 for biochar fuels, with the value varying with the sulfur content in the fuel [94]. Nitrogen volume produced, V_{N2} constituted a significant fraction from inert N_2 (79 % v/v) in the air and when combusted, the N_2 gas is retained as part of the flue gases due to the non-reactive of inert N_2 molecules at combustion temperatures (<1500 ℃). Also, the demineralized biochar constituted a small fraction of N_2 at 2.95 % (Sub-section 4.3.1) and this N_2 constitutes bond structures in the biochar and during combustion, they disintegrate to form NO_X emissions, which contribute to the GHGs [103]. Argon volume, V_{Ar}, composition is equivalent to the Ar content in the air. At combustion temperatures, Ar is non-reactive [104]. The $V_{DFG,min}$ was 5.266 $Nm^3\ kg^{-1}$ fuel. The CO_{2max} in the flue gas is 20.95 % and Jakub Vrana [105] reported a similar percentile range when the author determined it for wood chips. The minimum amount of water vapor ($V_{H2O,min}$) in the flue gas is 0.605 $Nm^3\ kg^{-1}$ fuel. This value arises from the moisture content in the biochar and the combustion air.

Our findings have low moisture vapor in the flue gas, indicating that the moisture in the biochar has an insignificant effect on the combustion efficiency and temperature profile. In addition, literature [45,94] indicates a $V_{H2O,min}$ ranging between 0.500 – 0.800Nm^3kg^{-1} fuel, can be produced in the stoichiometric combustion when biomass is combusted.

Table 10 Stoichiometric flue gas production from a kilogram of demineralized biochar

Parameter	Symbol	Amount
The volume of carbon dioxide	V_{CO2}	1.209 $Nm^3\ kg^{-1}$ fuel
Volume of Sulphur dioxide	V_{SO2}	0.003 $Nm^3\ kg^{-1}$ fuel
Volume of Nitrogen	V_{N2}	4.007 $Nm^3\ kg^{-1}$ fuel
Volume of Argon	V_{Ar}	0.047 $Nm^3\ kg^{-1}$ fuel
Minimum volume of dry flue gases	$V_{DFG,min}$	5.266 $Nm^3\ kg^{-1}$ fuel
The maximum amount of Carbon dioxide in flue gas	CO_{2max}	20.95 %
Minimum amount of water vapor	$V_{H2O,min}$	0.605 $Nm^3\ kg^{-1}$ fuel
Minimum amount of wet flue gases	$V_{WFG,min}$	5.871 $Nm^3\ kg^{-1}$ fuel
Actual amount of flue gas	$V_{FG,act}$	7.176 $Nm^3\ kg^{-1}$ fuel
Flue gas exit temperature (Section 3.3.3)	T_{FG}	503.75 ℃
Density of the flue gas	ρ_{FG}	0.454 kg m^{-3}
Actual mass of flue gas produced	$m_{FG,act}$	3.257 kg kg^{-1} fuel

The minimum amount of wet flue gases ($V_{WFG,min}$) is 5.871 $Nm^3\ kg^{-1}$ fuel. This includes the contributions from both dry gases and water vapor. The actual amount of flue gas ($V_{FG,act}$) produced is 7.176 $Nm^3\ kg^{-1}$ fuel. The density of flue gas (ρ_{FG}) is 0.454 kg $m^{-3,}$ which corresponds to the average burnout temperature (503.75 °C, Section 3.3) of the demineralized biochar—calculated the actual mass of flue gas ($m_{FG,act}$) to be 3.26 kg kg^{-1} fuel.

3.9. Enthalpy of air and flue gases

The enthalpy of air and flue gases are critical in determining the thermal efficiency and performance in a combustion system. Figure 7 shows the results of the enthalpy of air and the enthalpy of flue gases at stoichiometric conditions and at 25 % excess air. The humidity ratio (ω) was calculated to be 14.17, which was then used to determine the specific heat capacity of humid air ($C^T_{P,ha}$). The demineralized biochar ash content (AC) is 18.63 % (Section 3.1) and at a 30 % worst-case scenario of fly ash (FA) composition retained in the biochar AC, the biochar produced 5.59 % of the FA.

The FA was applied to determine the AC inequality, $AC > \frac{6 \times LHV_{ar}}{41.8 \times FA}$ which was not satisfied (18.63 %>55.09 %), hence the enthalpy of fly ash was not considered in determining the enthalpy of flue gas at stoichiometric enthalpy (h^T_{FG}) and enthalpy at 25 % excess air ($h^T_{FG,\alpha=1.25}$) under a varying temperature range of 100 – 800 °C with the results shown in Figure 7.

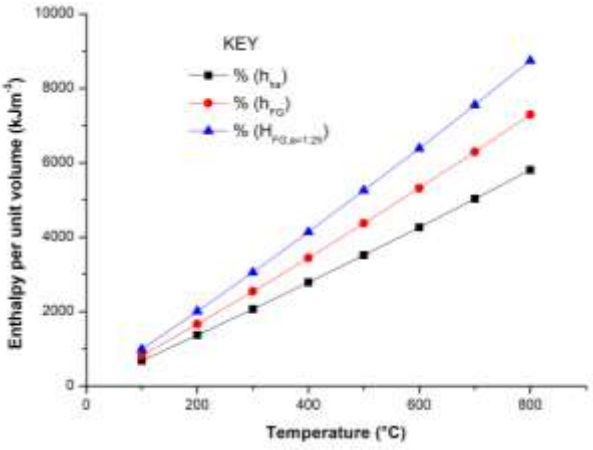

Fig 7 Enthalpy of air and flue gas at stoichiometric and 25 % excess air per unit volume

As shown in Figure 7, an increase in temperature resulted in a direct linear increase in all the enthalpies with $h^T_{FG,\alpha=1.25} > h^T_{FG} > h^T_{ha}$, with the enthalpy of air (h^T_{ha}) being observed to be lower across the temperature profile. The low enthalpy values of h^T_{ha} show that low thermal energy is introduced through air for igniting the biochar, which is less than the energy generated during combustion and carried by the flue gas. At stoichiometric conditions, the enthalpy of flue gas (h_{FG}) is observed to be lower than that with 25 % excess air ($h^T_{FG,\alpha=1.25}$). More thermal energy is carried by the excess air that also constitutes part of the flue gases. Also, the $h_{FG,\alpha=1.25}$ has a steeper slope compared to h_{FG}, indicating a higher rate of enthalpy increase with temperature and a significant heat loss via the flue gases, hence reducing the combustion efficiency. Excess air affects the thermal efficiency of the combustion process. Vrana [105] reported that excess air that goes beyond 30 % in biomass combustion results in the decline of the thermal efficiency, as the flow rate of heat leaving the chamber will be high.

3.10. Efficiency of the combustion chamber

Table 11 shows the results for the thermal losses and overall combustion efficiency of biochar derived from demineralized PL for firing in an FBCC. The combustion efficiency is 86.20 %, with the balance of heat losses caused by the loss due to flue gases (L1), loss due to hydrogen loss in fuel (L2), loss due to moisture in fuel (L3), loss due to moisture in air (L4) and loss due to unburnt carbon (L5).

Table 11 Thermal efficiency loss of biochar in a combustion chamber

Loss	Symbol	Thermal loss (%)
Flue gases	L1	7.30
Hydrogen	L2	4.45
Moisture in fuel	L3	0.00
Moisture in the air	L4	0.57
Unburnt carbon	L5	1.48
Overall thermal efficiency	η	86.20

Heat loss due to flue (L1) is the highest at 7.30 % among the other heat losses. This is caused by sensible heat exiting the combustion chamber with the combustion products (H_2O and CO_2). Other literature notes that heat loss due to flue gases on biochar fuels ranges between 7 – 12 % when fired in the FBCC [44,64]. This shows that biochar in the study, when fired in an FBCC, will produce L1 that is deemed to be in the tolerance range with the literature range on similar fuel. However, improving the bed material heat recovery and optimizing the air-to-fuel ratio will greatly reduce the L1 loss.

The loss due to hydrogen in fuel (L2) is the second highest at 4.45 %. The hydrogen causes this loss in the biochar, which, during combustion, oxidizes with oxygen to form water vapor, which loses energy through the latent heat of vaporization [106]. Other studies [107,108] that utilized biochar as a fuel reported a loss due to hydrogen ranging between 1 – 5 %. Our study aligns with the literature on the loss due to hydrogen in fuel.

Heat loss due to moisture in the fuel (L3) is 0 %, which is undetectable. In relation to the biochar in the study, the moisture content is undetectable (0 %), hence

not contributing to the heat sink [66]. Loss due to moisture in the air (L4) is 0.57 %, showing that the moisture in the air is low. Such a minimal loss is expected and aligns with the ideal scenarios where the air used for combustion is adequately dehumidified [109].

The unburnt carbon ($C_{unburnt}$) that constitutes 5.20 % with reference to the fixed carbon (FC) composition was used in determining the loss due to unburnt carbon (L5). The L5 was noted at 1.48 %, which is significantly low and is within the loss due to the unburnt carbon range of 0.50 – 2.00 % for the fluidized bed combustion chambers [110]. The overall efficiency of 86.20 % is quite high, demonstrating effective combustion and heat utilization within the combustion chamber. This efficiency is competitive when compared to other biomass combustion systems [60].

4. Conclusions

The biochar derived from demineralized PL improved its physicochemical properties compared to biochar derived from undemineralized PL. An increase in the TGA/DTG heating rate (5 – 20 °C min^{-1}) shifted the reaction region to high temperature (58.57-548.93 °C), increasing peak temperatures and their DTG_{max} points, signifying a reduction in ease to ignite and combust. Low activation energy (E_a) was observed with a small difference between E_a and enthalpy (H) -2.27 kJ $mol^{-1,}$ showing the dominance of C–C and C–O linkages during combustion. The biochar has a high fouling and slagging tendency, but its ash melting point is high. The fluidised bed combustion chamber is better suited for the developed biochar. For stoichiometric conditions, 7.830 kg kg^{-1} fuel of mass of air is required to combust a kilogram of biochar to produce 3.257 kg kg^{-1} fuel of flue gas. The enthalpy of flue gas at 25 % excess shows a balance on maintaining energy while attaining 86.20 % thermal efficiency. The biochar from demineralized PL has better properties than biochar from undemineralized PL and combusts better at low heating rates.

List of Symbols

A	Arrhenius constant or pre-exponential factor
Al	Alkali index/Mile index
$CO_{2,max}$	The maximum amount of Carbon dioxide in flue gas
E_a	Activation energy
f_{corr}	Air correction factor.
Fu	Fouling index
ΔG	Gibbs free energy change
ΔH	Enthalpy change
$m_{A,act}$	Actual mass of air per kilogram of biochar fuel
$m_{FG,actual}$	Actual mass of flue gases produced per kilogram of biochar fuel
m_{H_2O}	Mass flow rate of water
P_{ha}	Absolute pressure of humid air
P_{SV}	Saturated vapor pressure
R	Universal gas constant
$R_{b/a}$	Base-to-acid ratio
R_s	Slagging/Babcock index
Sr	Slagging ratio
Si/Al	Silica–to–Aluminum ratio
T	Absolute temperature
T_a	Air inlet temperature
T_b	Burnout temperature
Ti	Ignition temperature
T_p	Peak temperature
h	Planck Constant
h_{ha}^{T}	Enthalpy of humid air
h_{FA}^{T}	Enthalpy of fly ash
h_{FG}^{T}	Enthalpy of flue gas
$h_{FG,min}^{T}$	Minimum enthalpy of flue gases per unit volume
k_B	Boltzmann constant
ΔS	Entropy change
$V_{A,act}$	Actual volume of air used to combust a unit of biochar fuel
V_{Ar}	Argon flue gas volume
V_{CO2}	Carbon dioxide flue gas volume
$V_{DA,min}$	Minimum volume of dry air
$V_{DFG,min}$	Minimum volume of dry flue gases
$V_{FG,act}$	Actual volume of flue gas
$V_{H2O,min}$	Minimum volume of water vapor
V_{H2O}	Water vapor at 1.00m^3 of dry air
V_{N2}	Nitrogen flue gas volume
$V_{O2,min}$	Minimum volume of oxygen to burn 1kg of fuel
$V_{RH,min}$	Minimum volume of relative humid air
V_{SO2}	Sulphur dioxide flue gas volume
$V_{WFG,min}$	Minimum amount of wet flue gases
ϕ	Equivalence ratio
α	Excess air ratio
β	Heating rate
η_{cc}	Combustion chamber efficiency
λ	Latent heat of vaporization
$\rho_{A,}$ ρFG	Density of air, flue gas density
ω	Humidity ratio

List of Abbreviations

AC	Ash content
BAI	Bed agglomeration index
CAGR	Compound annual growth rate
CF_{oxide}	Inorganic element oxide conversion factor

DTG_{max},	Maximum weight loss rate
DTG_{mean}	Average weight loss rate
D_b	Burnout index
D_c	Comprehensive performance index
D_i	Ignition index
FA	Fly ash content
FBCC	Fluidized bed combustion chamber
FC	Fixed Carbon
GFCC	Grate–Fired combustion chamber
GHGs	Greenhouse Gases
H/C ratio	Hydrogen–to–Carbon ratio
HHV_{db}	Higher heating value on a dry basis
ID	Internal diameter
L1	Heat loss in dry flue gases
L2	Heat loss in hydrogen in the fuel
L3	Heat loss due to moisture in the fuel
L4	Heat loss due to moisture in the air
L5	Heat loss due to unburnt carbon
LHV_{ar}	Lower heating Value as-received basis
MC	Moisture Content
O/C ratio	Oxygen–to–Carbon ratio
PCC	Pulverized combustion chamber
PL	Poultry Litter
RH	Relative humidity of air
T_{FG}	Flue gas exit temperature
TCD	Thermal conductivity detector
TGA/DTG	Thermogravimetric and differential thermogravimetric analysis
VM	Volatile matter
w/v	Weight–to–volume ratio
W_{oxide}	Inorganic element oxide

Availability of Supplementary Data

Supplementary data supporting the findings of this study are available from the corresponding author upon reasonable request.

Acknowledgments

The authors appreciate the technical assistance of Thato Mongalenyane from the Department of Mechanical, Energy & Industrial Engineering at Botswana International University of Science and Technology for his support in Laboratory analysis.

References

1. Satista, Forecast of the Total Population of Africa from 2021 to 2050, Satista (2024). https://www.statista.com/statitics/1224205/forecast-of-the-total-population-of-africa (accessed April 7, 2025).
2. Global Change Data Lab, Global primary energy consumption by source, Our World Data (n.d.).https://ouworldindata.org/grapher/global-energy-substitution.
3. I.E. Agency, CO2 Emissions in 2023, 2023.
4. Global Change Data Lab, Annual temperature anomalies relative to the pre-industrial period, World, Our World Data (n.d.). https://ourworldindata.org/grapher/temperature-anomaly?focus=~Average (accessed October 17, 2025).
5. C.A. Tracker, Emissions Pathways to 2100, (2024). https://climateactiontracker.org/global/emissions-pathways/ (accessed August 10, 2024).
6. C. in W. Farming, Information Sheet 1-Broiler Production-Global, 2023. https://www.compassioninfoodbusiness.com/media/7455890/info-sheet-1-broiler-production-global.pdf.
7. M.M. Rahman, A. Hassan, I. Hossain, M.M.R. Jahangir, E.H. Chowdhury, R. Parvin, Current state of poultry waste management practices in Bangladesh, environmental concerns, and future recommendations, J. Adv. Vet. Anim. Res. 9 (2022) 490–500. https://doi.org/10.5455/javar.2022.i618.
8. J. Zhang, A. Li, C. Zhang, C. Yang, Advances in poultry litter disposal technology-a review, J. Fail. Anal. Prev. 16 (2016) 302–309. https://doi.org/10.1007/s11668-016-0088-z.
9. A. Sharpley, N. Slaton, J. Tom Tabler, K. VanDevender, M. Daniels, F. Jones, T. Daniel, Nutrient Analysis of Poultry Litter, Environ. Sci. (2007) 1–6.
10. N.É. Kiss, J. Tamás, V. Mannheim, A. Nagy, Comparing the environmental impact of poultry manure and chemical fertilizers, Front. Built Environ. 9 (2023) 1–8. https://doi.org/10.3389/fbuil.2023.1237476.
11. P.J.A. Kleinman, A.N. Sharpley, P.J.A. Withers, L. Bergström, L.T. Johnson, D.G. Doody, Implementing agricultural phosphorus science and management to combat eutrophication, Ambio 44 (2015) 297–310. https://doi.org/10.1007/s13280-015-0631-2.
12. K.R. Sistani, J.R. Simmons, M. Jn-Baptiste, J.M. Novak, Poultry litter, biochar, and fertilizer effect on corn yield, nutrient uptake, N2O and CO2 emissions, Environ. - MDPI 6 (2019). https://doi.org/10.3390/environments6050055.
13. Melton Renewable Energy, Biomass and Feedstock, Melt. Renew. Energy (2023). https://www.mreuk.com/our-operations/biomass.
14. P. World, Poultry litter used to generate power as public anger grows, Poult. World (2023). https://www.poultryworld.net/the-industry-markets/market-trends-analysis-the-industry-markets-2/poultry-litter-used-to-generate-power-as-public-anger-grows.
15. Q. Ma, K.P. Paudel, D. Bhandari, C. Theegala, M. Cisneros, Implications of poultry litter usage for electricity production, Waste Manag. 95 (2019)

493–503. https://doi.org/10.1016/j.wasman.2019.06.022.
16. K. Nyoni, L. Kelebopile, Multivariate Optimization of Pyrolysis Process Parameters for Bi-Ochar Production Derived From Demineralized Poultry Litter Using Response Surface Methodology, Paliva 15 (2023) 101–115. https://doi.org/10.35933/paliva.2023.03.05.
17. S. Lehmann, J and Joseph, Biochar for Enviromental Mnanagement: Science, Technology and Implimentation, Routledge, London, 2015. https://doi.org/10.4324/9780203762264.
18. Y. Yang, X. Qian, S.O. Alamu, K. Brown, S.W. Lee, D.H. Kang, Qualities and Quantities of Poultry Litter Biochar Characterization and Investigation, Energies 17 (2024). https://doi.org/10.3390/en17122885.
19. S. Katuwal, A. Ashworth, N.-A.-S. Rafsan, P. Kolar, Characterization of Poultry Litter Biochar and Activated Biochar as a Soil Amendment for Valorization, Biomass 2 (2022) 209–223. https://doi.org/10.3390/biomass2040014.
20. A.G. Adeniyi, J.O. Ighalo, K.O. Iwuozor, M.A. Amoloye, A study on the thermochemical co-conversion of poultry litter and elephant grass to biochar, Clean Technol. Environ. Policy 24 (2022) 2193–2202. https://doi.org/10.1007/s10098-022-02311-3.
21. J.M. Novak, K.B. Cantrell, D.W. Watts, Compositional and Thermal Evaluation of Lignocellulosic and Poultry Litter Chars via High and Low Temperature Pyrolysis: High and Low Temperature Pyrolyzed Biochars, Bioenergy Res. 6 (2013) 114–130. https://doi.org/10.1007/s12155-012-9228-9.
22. W. Song, M. Guo, Quality variations of poultry litter biochar generated at different pyrolysis temperatures, J. Anal. Appl. Pyrolysis 94 (2012) 138–145. https://doi.org/10.1016/j.jaap.2011.11.018.
23. K. Nyoni, L. Kelebopile, Physio-chemical and Thermal Characterization of Demineralized Poultry Litter using Mechanical Sizing Fractioning, Acid Solvents, and Deionized Water, J. Chem. Environ. 2 (2023) 82–96. https://doi.org/10.56946/jce.v2i2.153.
24. P. Shrivastava, A. Kumar, P. Tekasakul, S.S. Lam, A. Palamanit, Comparative investigation of yield and quality of bio-oil and biochar from pyrolysis of woody and non-woody biomasses, Energies 14 (2021) 1–23. https://doi.org/10.3390/en14041092.
25. M. Barbanera, F. Cotana, U. Di Matteo, Co-combustion performance and kinetic study of solid digestate with gasification biochar, Renew. Energy 121 (2018) 597–605. https://doi.org/10.1016/j.renene.2018.01.076.
26. I. Made Rajendra, I. Nyoman Suprapta Winaya, A. Ghurri, I. Ketut Gede Wirawan, Comprehensive kinetic study of pyrolysis of sunan candlenut: The effect of using iron oxide, zeolite and ZSM-5 as bed materials, Int. J. Heat Technol. 39 (2021) 493–502. https://doi.org/10.18280/ijht.390219.
27. L. Jeníček, B. Tunklová, J. Malaťák, J. Velebil, J. Malaťáková, M. Neškudla, F. Hnilička, The Impact of Nutshell Biochar on the Environment as an Alternative Fuel or as a Soil Amendment, Materials (Basel). 16 (2023). https://doi.org/10.3390/ma16052074.
28. P.C. Ani, H. Alhameedi, H.J. Al-abedi, H. Alrubaye, Z. Zeitoun, U. Ewuzie, J.D. Smith, The Comprehensive Quantification and Characterization of Oak Biochar Produced via a Gasification Process Using a Downdraft Reactor, (2025) 1–22.
29. [I. Gravalos, D. Kateris, P. Xyradakis, T. Gialamas, S. Loutridis, A. Augousti, A. Georgiades, Z. Tsiropoulos, A study on calorific energy values of biomass residue pellets for heating purposes, For. Eng. Meet. Needs Soc. Environ. (2010) 1–9. https://www.formec.org/images/proceedings/2010/ab066.pdf.
30. P. Basu, Biomass Gasification, Pyrolysis and Torrefaction: Practical Design and Theory, 2013. https://doi.org/10.1016/C2011-0-07564-6.
31. G.-B. Chen, J.-W. Li, H.-T. Lin, F.-H. Wu, Y.-C. Chao, A Study of the Production and Combustion Characteristics of Pyrolytic Oil from Sewage Sludge Using the Taguchi Method, Energies 11 (2018) 2260. https://doi.org/10.3390/en11092260.
32. S. Paniagua, L.F. Calvo, C. Escapa, R.N. Coimbra, M. Otero, A.I. García, Chlorella sorokiniana thermogravimetric analysis and combustion characteristic indexes estimation, J. Therm. Anal. Calorim. 131 (2018) 3139–3149. https://doi.org/10.1007/s10973-017-6734-1.
33. Y. Xu, B. Chen, Investigation of thermodynamic parameters in the pyrolysis conversion of biomass and manure to biochars using thermogravimetric analysis, Bioresour. Technol. 146 (2013) 485–493. https://doi.org/10.1016/j.biortech.2013.07.086.
34. J.J. Lu, W.H. Chen, Investigation on the ignition and burnout temperatures of bamboo and sugarcane bagasse by thermogravimetric analysis, Appl. Energy 160 (2015) 49–57. https://doi.org/10.1016/j.apenergy.2015.09.026.
35. C. Ulloa, A.G. Borrego, S. Helle, A.L. Gordon, X. García, Char characterization and DTF assays as tools to predict burnout of coal blends in power plants, Fuel 84 (2005) 247–257. https://doi.org/10.1016/j.fuel.2004.08.008.
36. X. Li, W. Miao, Y. Lv, Y. Wang, C. Gao, D. Jiang, TGA-FTIR investigation on the co-combustion characteristics of heavy oil fly ash and municipal sewage sludge, Thermochim. Acta 666 (2018) 1–9. https://doi.org/10.1016/j.tca.2018.05.023.
37. R.L. Blaine, H.E. Kissinger, Homer Kissinger and the Kissinger equation, Thermochim. Acta 540 (2012) 1–6. https://doi.org/10.1016/j.tca.2012.04.008.

38. M.S. Alfredsson, Effects of Different Fuels on Combustion Boiler Processes The analysis of alternative fuel mixtures, (2018) 59.
39. Element-to-stoichiometric oxide conversion factors, James Cook Univ. Aust. (n.d.). https://www.jcu.edu.au/advanced-analytical-centre/resources/element-to-stoichiometric-oxide-conversion-factors.
40. S. Feldmeier, E. Wopienka, M. Schwarz, C. Schön, C. Pfeifer, Applicability of Fuel Indexes for Small-Scale Biomass Combustion Technologies, Part 1: Slag Formation, Energy and Fuels 33 (2019) 10969–10977. https://doi.org/10.1021/acs.energyfuels.9b02409.
41. C. Thiel, Slagging and Fouling Behavior of Geramn lignites Based on the Association of Mineral Matter in Coal, (2018).
42. D. Silverstein, P. Samuel, N. Decarlo, Pugh Matrix, Innov. Toolkit (2008) 212–216. https://doi.org/10.1002/9781118258316.ch36.
43. C.L. Dym, P. Little, E.J. Orwin, Engineering design: a project-based introduction, 2002. https://doi.org/10.1016/s0261-3069(01)00050-4.
44. S. van Loo, J. Koppejan, The Handbook of Biomass Combustion and Cofiring, 2008.
45. A. Demirbas, Combustion characteristics of different biomass fuels, Prog. Energy Combust. Sci. 30 (2004) 219–230. https://doi.org/10.1016/j.pecs.2003.10.004.
46. J.M. Jones, L.I. Darvell, T.G. Bridgeman, M. Pourkashanian, A. Williams, An investigation of the thermal and catalytic behaviour of potassium in biomass combustion, Proc. Combust. Inst. 31 II (2007) 1955–1963. https://doi.org/10.1016/j.proci.2006.07.093.
47. L. Baxter, Biomass-coal co-combustion: Opportunity for affordable renewable energy, Fuel 84 (2005) 1295–1302. https://doi.org/10.1016/j.fuel.2004.09.023.
48. A.K. Joshi, I.A. Dandekar, M. V. Gaikwad, C.G. Harge, Pugh Matrix and Kano Model-The Significant Techniques for Customer"s Survey, Int. J. Emerg. Technol. Adv. Eng. 9 (2019) 53–55.
49. K.B. Cantrell, P.G. Hunt, M. Uchimiya, J.M. Novak, K.S. Ro, Impact of pyrolysis temperature and manure source on physicochemical characteristics of biochar, Bioresour. Technol. 107 (2012) 419–428. https://doi.org/10.1016/j.biortech.2011.11.084.
50. C. Gupta, Fuels, Furnaces and Refractories, PHI Learning, 1977. https://doi.org/10.1016/c2013-0-02746-6.
51. J. (Techincal U.B. Strecha, Grill Boiler for Biomass Combustion (Grate Biomass Boiler) 88T/H, 9.6MPa, 520°C, Technical University Brno, 2017.
52. M. Vojtek, Design of a Thermal Oil Boiler combusting wood chip, Technical University Brno, 2016.
53. J. Kitto, S. Stultz, Steam: Its generation and use, 2005.
54. L.D. Varanda, C. Roberto, S. Jr, F.M. Yamaji, Biochar produced from poultry litter waste, 2021 (2021) 1–13.
55. M. Lubwama, V.A. Yiga, F. Muhairwe, J. Kihedu, Physical and combustion properties of agricultural residue bio-char bio-composite briquettes as sustainable domestic energy sources, Renew. Energy 148 (2020) 1002–1016. https://doi.org/10.1016/j.renene.2019.10.085.
56. Z. Liu, B. Fei, Z. Jiang, X. Liu, Combustion characteristics of bamboo-biochars, Bioresour. Technol. 167 (2014) 94–99. https://doi.org/10.1016/j.biortech.2014.05.023.
57. A. Ndecky, P.W. Tavares, A. Senghor, M. Kane, H. Ndiath, I. Youm, Proximate Analysis of Alternatives Cooking Solides Fuels in Sub Saharan by Using Astm Standards, Int. J. Clean Coal Energy 11 (2022) 1–12. https://doi.org/10.4236/ijcce.2022.111001.
58. I.C. Kantarli, A. Kabadayi, S. Ucar, J. Yanik, Conversion of poultry wastes into energy feedstocks, Waste Manag. 56 (2016) 530–539. https://doi.org/10.1016/j.wasman.2016.07.019.
59. J.M. Lee, D.W. Kim, J.S. Kim, Reactivity study of combustion for coals and their chars in relation to volatile content, Korean J. Chem. Eng. 26 (2009) 506–512. https://doi.org/10.1007/s11814-009-0086-x.
60. A.A. Khan, W. de Jong, P.J. Jansens, H. Spliethoff, Biomass combustion in fluidized bed boilers: Potential problems and remedies, Fuel Process. Technol. 90 (2009) 21–50. https://doi.org/10.1016/j.fuproc.2008.07.012.
61. R.K. Mishra, K. Mohanty, Characterization of non-edible lignocellulosic biomass in terms of their candidacy towards alternative renewable fuels, Biomass Convers. Biorefinery 8 (2018) 799–812. https://doi.org/10.1007/s13399-018-0332-8.
62. K.E. Brantley, K.R. Brye, M.C. Savin, D.E. Longer, Biochar Source and Application Rate Effects on Soil Water Retention Determined Using Wetting Curves, Open J. Soil Sci. 05 (2015) 1–10. https://doi.org/10.4236/ojss.2015.51001.
63. W.H. Chen, J. Peng, X.T. Bi, A state-of-the-art review of biomass torrefaction, densification and applications, Renew. Sustain. Energy Rev. 44 (2015) 847–866. https://doi.org/10.1016/j.rser.2014.12.039.
64. T. Nussbaumer, Combustion and Co-combustion of Biomass: Fundamentals, Technologies, and Primary Measures for Emission Reduction, Energy and Fuels 17 (2003) 1510–1521. https://doi.org/10.1021/ef030031q.
65. A. Enders, K. Hanley, T. Whitman, S. Joseph, J. Lehmann, Characterization of biochars to evaluate recalcitrance and agronomic performance, Bioresour. Technol. 114 (2012) 644–653. https://doi.org/10.1016/j.biortech.2012.03.022.

66. B. Jenkins M., L. Bexter L., T. Miles R. Jr., T. Miles R., Combustion Properties of Biomass, Fuel Process. Technol. 54 (1998) 17–46.
67. J.S. Cha, S.H. Park, S.C. Jung, C. Ryu, J.K. Jeon, M.C. Shin, Y.K. Park, Production and utilization of biochar: A review, J. Ind. Eng. Chem. 40 (2016) 1–15. https://doi.org/10.1016/j.jiec.2016.06.002.
68. M.J. Antal, M. Grønli, The art, science, and technology of charcoal production, Ind. Eng. Chem. Res. 42 (2003) 1619–1640. https://doi.org/10.1021/ie0207919.
69. A. Demirbas, Effects of temperature and particle size on bio-char yield from pyrolysis of agricultural residues, J. Anal. Appl. Pyrolysis 72 (2004) 243–248. https://doi.org/10.1016/j.jaap.2004.07.003.
70. J.E. White, W.J. Catallo, B.L. Legendre, Biomass pyrolysis kinetics: A comparative critical review with relevant agricultural residue case studies, J. Anal. Appl. Pyrolysis 91 (2011) 1–33. https://doi.org/10.1016/j.jaap.2011.01.004.
71. S. Vyazovkin, A.K. Burnham, J.M. Criado, L.A. Pérez-Maqueda, C. Popescu, N. Sbirrazzuoli, ICTAC Kinetics Committee recommendations for performing kinetic computations on thermal analysis data, Thermochim. Acta 520 (2011) 1–19. https://doi.org/10.1016/j.tca.2011.03.034.
72. K.S. Ro, K.B. Cantrell, P.G. Hunt, High-temperature pyrolysis of blended animal manures for producing renewable energy and value-added biochar, Ind. Eng. Chem. Res. 49 (2010) 10125–10131. https://doi.org/10.1021/ie101155m.
73. A. V. Bridgwater, Review of fast pyrolysis of biomass and product upgrading, Biomass and Bioenergy 38 (2012) 68–94. https://doi.org/10.1016/j.biombioe.2011.01.048.
74. A. Sever Akdağ, A. Atimtay, F.D. Sanin, Comparison of fuel value and combustion characteristics of two different RDF samples, Waste Manag. 47 (2016) 217–224. https://doi.org/10.1016/j.wasman.2015.08.037.
75. M.B. Ahmed, J.L. Zhou, H.H. Ngo, W. Guo, Insight into biochar properties and its cost analysis, Biomass and Bioenergy 84 (2016) 76–86. https://doi.org/10.1016/j.biombioe.2015.11.002.
76. D. López-González, M. Fernandez-Lopez, J.L. Valverde, L. Sanchez-Silva, Kinetic analysis and thermal characterization of the microalgae combustion process by thermal analysis coupled to mass spectrometry, Appl. Energy 114 (2014) 227–237. https://doi.org/10.1016/j.apenergy.2013.09.055.
77. M. Almazrouei, I. Janajreh, Thermogravimetric study of the combustion characteristics of biodiesel and petroleum diesel, J. Therm. Anal. Calorim. 136 (2019) 925–935. https://doi.org/10.1007/s10973-018-7717-6.
78. L.C. d. Morais, A.A. Maia, P.R. Resende, A.H. Rosa, L.J.R. Nunes, Thermochemical Conversion of Sugarcane Bagasse: A Comprehensive Analysis of Ignition and Burnout Temperatures, Clean Technol. 4 (2022) 1127–1137. https://doi.org/10.3390/cleantechnol4040068.
79. G. Várhegyi, M.J. Antal, E. Jakab, P. Szabó, Kinetic modeling of biomass pyrolysis, J. Anal. Appl. Pyrolysis 42 (1997) 73–87. https://doi.org/10.1016/S0165-2370(96)00971-0.
80. S. Wang, G. Dai, H. Yang, Z. Luo, Lignocellulosic biomass pyrolysis mechanism: A state-of-the-art review, Prog. Energy Combust. Sci. 62 (2017) 33–86. https://doi.org/10.1016/j.pecs.2017.05.004.
81. H.L. Friedman, Kinetics of thermal degradation of char-forming plastics from thermogravimetry. Application to a phenolic plastic, J. Polym. Sci. Part C Polym. Symp. 6 (1964) 183–195. https://doi.org/10.1002/polc.5070060121.
82. S. Duzyol, C. Sensogut, Investigation of the Thermal Improvement and the Kinetic Analysis of the Enriched Coal, J. Combust. 2018 (2018). https://doi.org/10.1155/2018/1761023.
83. C. Fushimi, K. Araki, Y. Yamaguchi, A. Tsutsumi, Effect of heating rate on steam gasification of biomass. 2. Thermogravimetric-mass spectrometric (TG-MS) analysis of gas evolution, Ind. Eng. Chem. Res. 42 (2003) 3929–3936. https://doi.org/10.1021/ie0300575.
84. L.A. Pérez-Maqueda, P.E. Sánchez-Jiménez, J.M. Criado, Kinetic analysis of solid-state reactions: Precision of the activation energy calculated by integral methods, Int. J. Chem. Kinet. 37 (2005) 658–666. https://doi.org/10.1002/kin.20115.
85. L. Álvarez, M. Gharebaghi, M. Pourkashanian, A. Williams, J. Riaza, C. Pevida, J.J. Pis, F. Rubiera, CFD modelling of oxy-coal combustion in an entrained flow reactor, Fuel Process. Technol. 92 (2011) 1489–1497. https://doi.org/10.1016/j.fuproc.2011.03.010.
86. C. Chen, Y. Bi, Y. Huang, H. Huang, Review on slagging evaluation methods of biomass fuel combustion, J. Anal. Appl. Pyrolysis 155 (2021) 105082. https://doi.org/10.1016/j.jaap.2021.105082.
87. Dan Boström, Markus Boström, Nils Skoglund, Christoffer Boman, Rainer Backman, Marcus Öhman, Alejandro Grimm, Ash transformation chemistry during energy conversion of biomass , Proc. Int. Conf. Impact Fuel Qual. Power Prod. Environ. (2010) 85–93. http://pure.ltu.se/portal/en/publications/ash-transformation-chemistry-during-energy-conversion-of-biomass(fe6a22f0-b78b-11df-a707-000ea68e967b).html.
88. J.Y. Malchi, R.A. Yetter, T.J. Foley, S.F. Son, The effect of added Al2O3 on the propagation behavior of an Al/CuO nanoscale thermite, Combust. Sci. Technol. 180 (2008) 1278–1294. https://doi.org/10.1080/00102200802049471.
89. D.J. Vega-Nieva, Slagging and Fouling Risks Derived from the Combustion of Solid Biofuels, 85 (2015) 137–147. https://doi.org/10.2495/978-1-84566-062-8/008.

90. P.P. Plaza, Fouling, The Development of a Slagging and Scale, Predictive Methodology for Large With, Pulverised Boilers Fired Blends, Coal/Biomass, Cardiff Sch. Eng. (2013) 227.
91. G. Zajac, J. Szyszlak-barglowici, Ash Composition and Deposition Tendencies of Selected Biomass Types, (2017) 438–443. https://doi.org/10.24326/fmpmsa.2017.79.
92. J. Lachman, M. Baláš, M. Lisý, H. Lisá, P. Milčák, P. Elbl, An overview of slagging and fouling indicators and their applicability to biomass fuels, Fuel Process. Technol. 217 (2021). https://doi.org/10.1016/j.fuproc.2021.106804.
93. D. Kunii, O. Levenspiel, Fluidization engineering, Powder Technol. 74 (1993) 197. https://doi.org/10.1016/0032-5910(93)87011-c.
94. D.A. Tillman, The Combustion of Solid Fuels and Wastes, 2012.
95. W. Yang, A. Ponzio, C. Lucas, W. Blasiak, Performance analysis of a fixed-bed biomass gasifier using high-temperature air, Fuel Process. Technol. 87 (2006) 235–245. https://doi.org/10.1016/j.fuproc.2005.08.004.
96. I. Pavel, R.I. Rădoi, G. Matache, A.M.C. Popescu, K. Pavel, Experimental Research to Increase the Combustion Efficiency in the Top-Lit Updraft Principle Based Gasifier, Energies 16 (2023). https://doi.org/10.3390/en16041912.
97. T. Bin Nur, M. Zafran Hanif, R. Purnomo Wibowo, M. Sembiring, Experimental Study of Combustion Chamber Performance Utilizing Biochar from Empty Fruit Bunch (EFB) as Fuel with Variation in Excess Air, E3S Web Conf. 519 (2024) 4–7. https://doi.org/10.1051/e3sconf/202451901001.
98. R.L. Bain, R.P. Overend, Biomass for heat and power, Int. Renew. Energy Agency 52 (2021) 12–19.
99. S.R. Turns, An Introduction to Combustion: Concepts and Applications, 2nd ed., McGraw-Hill, New York, 2013.
100. M. Balazi, Grate Boiler For Biomass and Coal Co-Combustion, 2014.
101. M. Pasteka, Design of a Grill Boiler for the Incineration of Sorted Waste, 2014.
102. M.L. de Souza-Santos, Solid Fuels Combustion and Gasification, Solid Fuels Combust. Gasif. (2004). https://doi.org/10.1201/9780203027295.
103. H. Lu, L.L. Baxter, Biomass Combustion Characteristics and Implications for Renewable Energy, in: Green Energy Technol., 2011: pp. 95–121. https://doi.org/10.1007/978-1-84996-393-0_5.
104. K. Savolainen, Co-firing of biomass in coal-fired utility boilers, Appl. Energy 74 (2003) 369–381. https://doi.org/10.1016/S0306-2619(02)00193-9.
105. J. Vrana, Grill Boiler for Chimney and Contaminated Biomass Combustion 50T/h, 2014.
106. . Basu, Circulating fluidized bed boilers: Design, operation and maintenance, 2015. https://doi.org/10.1007/978-3-319-06173-3.
107. M. V. Gil, D. Casal, C. Pevida, J.J. Pis, F. Rubiera, Thermal behaviour and kinetics of coal/biomass blends during co-combustion, Bioresour. Technol. 101 (2010) 5601–5608. https://doi.org/10.1016/j.biortech.2010.02.008.
108. D. Vamvuka, Thermal behavior of lignite and biomass blends during co-combustion, Fuel Process. Technol. 82 (2003) 79–92.
109. Gaur Siddhartha, T.B. Reed, Thermal data for natural and synthetic fuels, 1998.
110. Prabir Basu, Biomass Gasification and Pyrolysis: Practical Design and Theory, Academic Press, 2010.